ELECTRON TEMPERATURE MEASUREMENTS

IN AN ARGON/CESIUM PLASMA DIODE

THESIS

Michael J. Ward
Second Lieutenant, USAF

AFIT/GEP/ENP/87D-9

DEPARTMENT OF THE AIR FORCE
AIR UNIVERSITY
AIR FORCE INSTITUTE OF TECHNOLOGY

Wright-Patterson Air Force Base, Ohio

88 2 4 042

ELECTRON TEMPERATURE MEASUREMENTS

IN AN ARGON/CESIUM PLASMA DIODE

THESIS

Michael J. Ward
Second Lieutenant, USAF

AFIT/GEP/ENP/87D-9

Approved for public release; distribution unlimited.

AFIT/GEP/ENP/87D-9

ELECTRON TEMPERATURE MEASUREMENTS

IN AN ARGON/CESIUM PLASMA DIODE

THESIS

Presented to the Faculty of the School of Engineering

of the Air Force Institute of Technology
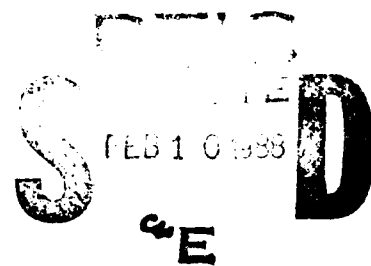
Air University

In Partial Fulfillment of the

Requirements for the Degree of

Master of Science in Engineering Physics

Michael J. Ward, B.S.
Second Lieutenant, USAF

December 1987

Accession For		
NTIS GRA&I		☒
DTIC TAB		☐
Unannounced		☐
Justification		
By		
Distribution/		
Availability Codes		
Dist	Avail and/or Special	
A-1		

Approved for public release; distribution unlimited

Acknowledgements

This study was by no means an individual effort. Instead it represents the commitment and hard work of several individuals. In particular, I thank Dr. William Bailey, my faculty advisor, for his patient effort in assisting me to understand the physics of plasmas and for helping me to address the difficult questions that arose in the course of this study. I also thank Dr. Biswa Ganguly, my laboratory advisor, who provided the conceptual and procedural basis for this study and who was always most willing to help. I owe thanks to Dr. S. Douglas Marcum and Mr. Mark Gieske, both of Miami University at Oxford, OH, for designing, constructing, and trouble-shooting the experimental apparatus and for providing important advice. I extend my gratitude to the the personnel of the Advanced Plasma Research Group, for their expertise and support. I also express my sincere thanks to my family and friends for their prayers and encouragement. But most of all, I wish to acknowledge the LORD, because He has been my strength and my hope through all of this.

Table of Contents

iv

List of Figures

List of Tables

Abstract

Line intensity measurements in an argon/cesium plasma diode were made at various locations within the discharge, yielding a spatially resolved electron temperature distribution. This device operated at 0.9 Torr argon, 0.04 Torr cesium, and at a current density of 1.05 mA/cm^2. Observations of the spectral line intensities of the $6P \rightarrow nS$ and $6P \rightarrow nD$ transitions of cesium yielded an average electron temperature of 8200 K throughout most of the discharge region. In contrast, the argon line emission data yields an average electron temperature of 13500 K. The difference between these two measured electron temperatures suggests that the electron energy distribution function is non-Maxwellian under the measured plasma conditions.

ELECTRON TEMPERATURE MEASUREMENTS
IN AN ARGON/CESIUM PLASMA DIODE

I. Introduction

Objective

Selection of the proper plasma diagnostic is crucial to
any examination of plasma phenomena. Hence, as the Advanced
Plasma Research Group at the Air Force Wright Aeronautical
Laboratories (AFWAL) began a study of the behavior of
argon/cesium plasmas, it was first necessary to select and
test a diagnostic method. In pursuit of this goal, this
present study employs spectral intensity measurements as a
means to characterize the electron energy distribution in an
argon/cesium diode.

The device examined consisted of two 2.54 cm diameter
molybdenum electrodes separated by a 1.8 cm gap. Due to the
onset of discharge instabilities at higher gas pressures and
current densities, the device was operated at 0.9 Torr
argon, 0.04 Torr cesium, and at a current density of 1.05
mA/cm². Due to the small dimension of the inter-electrode
gap, insertion of an electrostatic probe for diagnostic
purposes would dirupt discharge behavior. For this reason,
the non-intrusive character of spectral diagnostics is
attractive. Additionally, a spectral analysis yields
information of the gas composition. This information is

useful in comparing the relative effects of argon and cesium in the discharge. We now take a closer look at the expected behavior of such a device.

Background

The primary mechanism by which gas discharges are sustained is release of electrons from the cathode surface due to ion bombardment. The ejected electron creates electron-ion pairs as it moves towards the anode. In turn, the newly created ions are accelerated back to the cathode. When the ion flux at the cathode is sufficient to eject one replacement electron, the ionization process is continued and the discharge is said to be self-maintaining.

A close examination of a gas discharge reveals much more structure than accounted for in the above explanation. As an example, Figure 1 displays the general structure of the gas discharge. The various regions may be broken down as follows:

(A) Aston's dark space is the region in which the electrons are being accelerated by the applied field but do not yet have enough energy to ionize or excite any gas species.

(B) The first cathode layer is the region in which the electrons have acquired sufficient energy to excite. Depending on the structure of the gas atom, several such layers may exist.

(C) The cathode dark space evidences continued
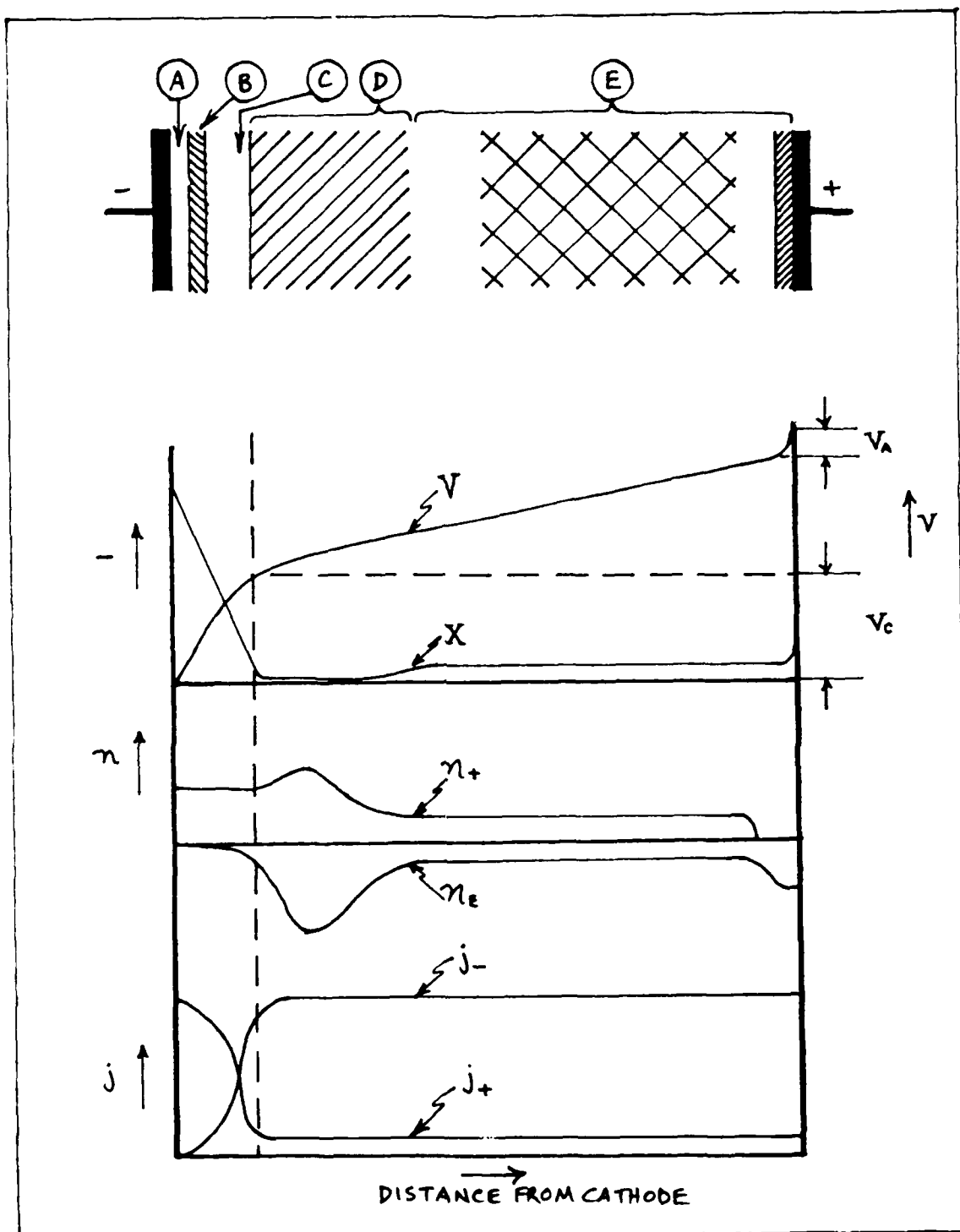
FIG. 1: General features of a glow discharge, where X is
the electric field, n+ and n- the space charge
densities, and j+ and j- the current densities.
(Ref. 1:218)

3

acceleration of the electrons. At this point they have surpassed the excitation energy and so ionization becomes the dominant process. As the electrons near the far boundary of this region, they have experienced nearly the entire cathode fall voltage, thereby giving them beam-like properties.

(D) In the negative glow, ionization processes continue but there are also sufficient numbers of slower electrons to initiate excitation as well. This highly non-equilibrium region marks the transition from a beam-like distribution to a thermalized distribution. Figure 2 displays the shift of the electron energy distribution from higher to lower energies as the electrons penetrate further into the negative glow region. However, one notes that if the peaks of these distributions can be described by a characteristic temperature, then the negative glow has two groups of electrons--a "fast" beam-like group, which is characterized by a large electron temperature, and a "slow" thermalized group, which is characterized by a smaller electron temperature.

By operating the discharge in argon (threshold energy >13 eV) and cesium (threshold energy <1 eV) we might sample both electron groups. Argon will only be sensitive to the fast electrons while cesium is more likely to inter-act with the slow electrons. Therefore an analysis of the argon spectrum might yield a different electron temperature than measured by an analysis of the cesium spectrum.

4
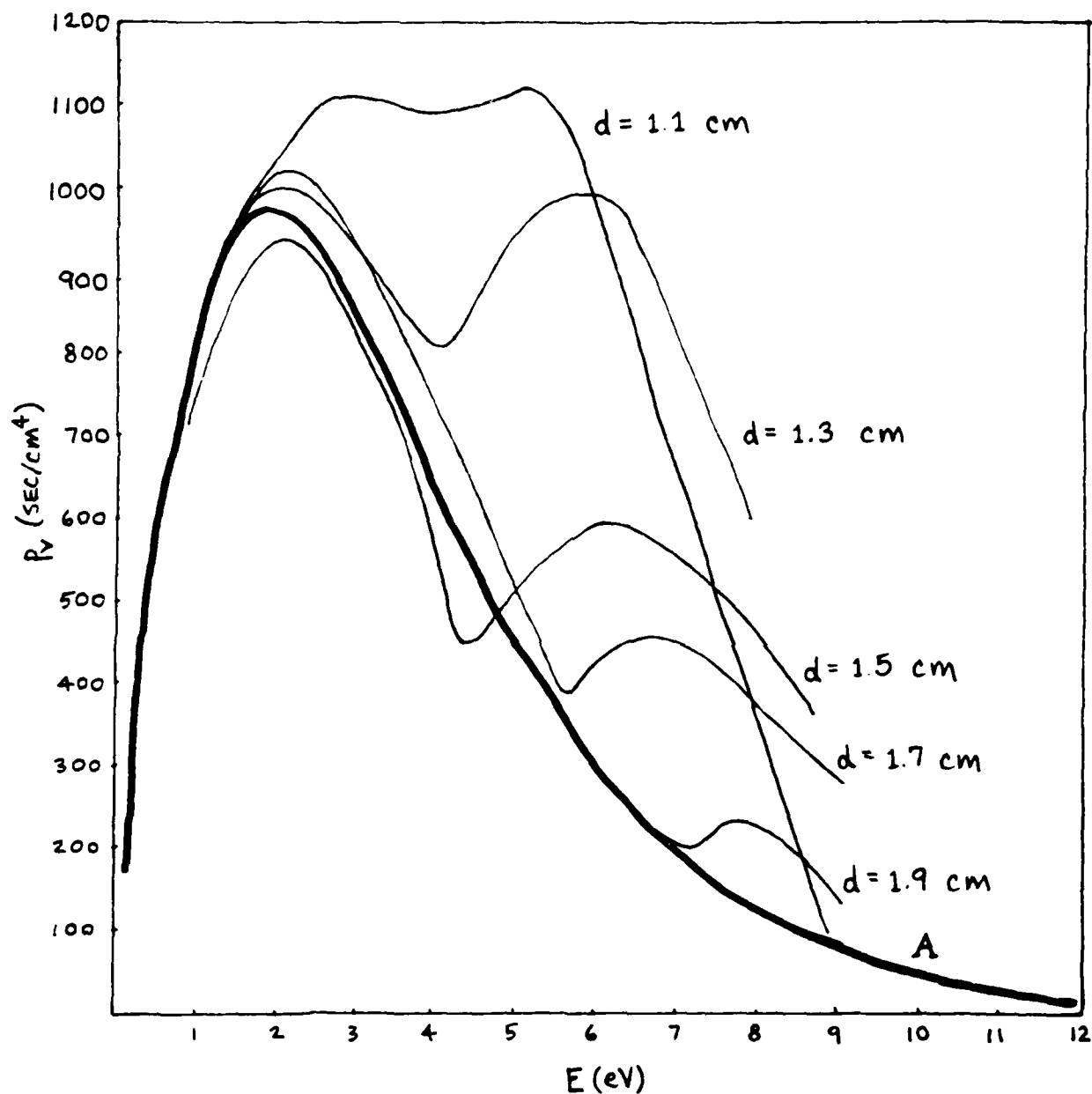
FIG. 2: Electron velocity distribution in the negative
glow and Faraday dark space of a neon discharge
operating at a current of 1.8 A, with a tube
diameter of 2.8 cm, and a pressure of 4.7 Torr.
Curve "A" is a Maxwellian which represents the
thermalized electrons. d is the distance from
the cathode.   (Ref. 2:207)

5

In order to establish relevant scale lengths for the discharge sheath structure and relate these to the present discharge geometry, we review the work of Brewer and Westhaver (Ref. 3:779). They measured the lengths of the negative glow region in various gases, for a variety of pressures and cathode fall voltages. Their results are shown in Figure 3. Examination of the argon curve for a cathode fall voltage of 200 volts establishes the length of the negative glow to be 1 cm. Considering the dimemsions of the device used in this study, we expect to be dealing with an obstructed discharge (Ref. 1:234). The highly non-equilibrium and beam-like structure of the electron energy distribution should be reflected in the spectroscopic observations.

(E) If the electrode separation is larger than the sheath dimensions, a positive column will be formed. However, since the gap is nearly the same size as the expected length of the negative glow, it is doubtful that the remaining discharge regions would be established.

Order of Presentation

Having discussed general discharge behavior, Chapter II of this report examines the theoretical framework around which the spectral diagnosis of such a discharge is built. This consists of a detailed comparison of the various discharge processes which results in the derivation of a relationship between spectral intensity and the electron temperature. Chapter III describes the experimental

6
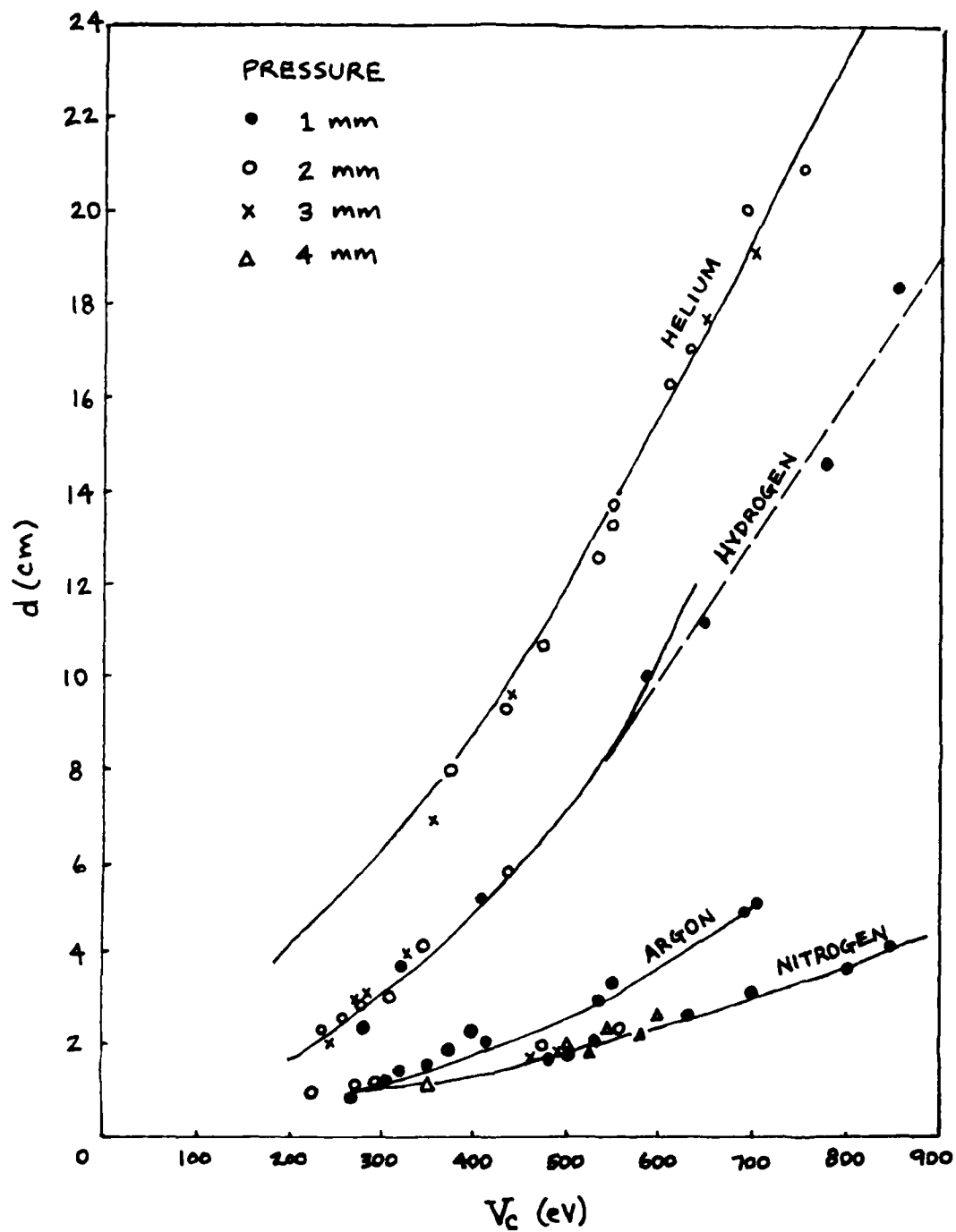
FIG. 3: Length of negative glow for various values
of the cathode fall in various gases.
(Ref. 3:779)

apparatus and Chapter IV explains the method by which this apparatus was used to gather data. A description of the data analysis and quantifiable results is presented in Chapter V, from which conclusions and recommendations are made in Chapter VI.

II. Theory of Extracting the Electron Temperature
From Line Intensity Measurements

The electron temperature, T_E , is a measure of the average kinetic energy of the electrons present in a discharge. If the dominant form of excitation in the the discharge is electron impact and if radiation is the primary decay mechanism, then we see that the excited state populations are linked to the energy distribution, $f(E)$, of free electrons. If the distribution is a Maxwellian that peaks near $E = E_U$ and has a smaller value at $E = E_L$, then one would expect the electron impact excitation of the upper level to be enhanced over the excitation of the lower level. Therefore, the radiative decay of these states should reveal a similar enhancement of the intensity of those lines which are characteristic of E_U over those which are characteristic of E_L . A measurement of the line intensities will then be a direct means of probing the electron energies and the corresponding electron temperatures.

But by neglecting the other mechanisms of excitation and decay, this description has been overly simplified. The following discussion remedies this situation by analyzing the various processes which alter the population of state E_U^- . These are incorporated into a rate equation, and the significance of each term is examined. This examination reveals that the assumption regarding the dominant discharge processes is well justified for the discharge which was studied. Solving the resultant equation in a steady state

9

relates measurement of spectral intensities to a value for T_E .

The Rate Equation

The mechanisms by which the upper state can be populated include electron impact excitation and recombination. Therefore the upper state is populated according to the rate $(dN_u/dt)_+$, where

$$\left(\frac{dN_u}{dt}\right)_+ = \langle R_{EXC} \rangle\, n_o n_E + \langle R_{REC} \rangle\, n_+ n_E$$

(1)

$\langle R_{EXC} \rangle$ is the frequency of electron impact excitation, and $\langle R_{REC} \rangle$ is the frequency of the recombination of free electrons. n_o , n_+ , and n_E are respectively the neutral, ion , and electron number densities.

The population of the excited state is depleted by radiative losses, electron collision de-excitation, and quenching collisions with heavy neutrals at the rate $(dN_u/dt)_-$, which is given by

$$\left(\frac{dN_u}{dt}\right)_- = N_u\left(A_{u1} + A_{u2} + A_{u3} + \cdots\right) + \langle R_Q \rangle\, n_o n_E + \langle R_{DEXC} \rangle\, n_E N_u$$

(2)

where A_{uL} is the spontaneous transition rate coefficient from a state with energy E_u to some lower state with energy E_L , $\langle R_Q \rangle$ is quenching collision frequency, and $\langle R_{DEXC} \rangle$ is the frequency of electron impact de-excitation.

In a steady-state, $(dN_u/dt)_+ = (dN_u/dt)_-$. Using this condition and Equations (1) and (2), N_u is solved for:

10

$$N_u = \frac{\langle R_{EXC} \rangle n_0 n_E + \langle R_{REC} \rangle n_+ n_E}{\sum_L A_{uL} + \langle R_Q \rangle n_0 + \langle R_{DEXC} \rangle n_E} \qquad (3)$$

The intensity I_{uL} of the transition from state u to state l is expressed by

$$I_{uL} = N_u A_{uL} (E_u - E_L) \qquad (4)$$

Hence, Equation (3) may be rewritten as

$$I_{uL} = N_u A_{uL} (E_u - E_L) \frac{\langle R_{EXC} \rangle n_0 n_E + \langle R_{REC} \rangle n_+ n_E}{\sum_L A_{uL} + \langle R_Q \rangle n_0 + \langle R_{DEXC} \rangle n_E} \qquad (5)$$

Now take a closer look at each of the terms in this equation.

Analysis of Discharge Processes

Electron Impact Excitation. One of the means of populating an excited state is by electron impact excitation from lower lying levels. In Equation (5), this contribution is expressed as $\langle R_{EXC} \rangle n_0 n_E$. $\langle R_{EXC} \rangle$ is obtained by integrating the product of the distribution function f(v) and R_{EXC} ($= Q_{EXC} v$) over all electron velocities, where Q_{EXC} is the excitation cross section:

$$\langle R_{EXC} \rangle = \int_0^\infty Q_{EXC}(\vec{v}) \cdot \vec{v} \cdot f(\vec{v}) \, d\vec{v} \qquad (6)$$

Zapesochnyi, et al., measured excitation cross-sections in both argon (Ref. 4:291) and cesium (Refs. 5:421, 6:6,

11

7:504). Tables I and II tabulate the maximum value of the cross section, Q_{MAX}, and the corresponding energy, E_{MAX}. To a good approximation, the excitation cross section varies linearly near the threshold energy. Hence, in the following treatment, $Q_{EXC}(E)$ is modeled as a linear function.

Upon viewing the cesium cross section data, one notes that Q_{MAX} is reached within only 1 eV of threshold. Since the cross section falls as ~1/E for electron energies greater than 1 eV, the linear approximation is no longer valid. However, we expect the thermal electrons, to which cesium is most sensitive, to have energies of less than 1 eV. We will se that the results of this study satisfy this expectation.

Literature values for the excitation cross section for the $4D_{1/2}°$ and $7S_{3/2}°$ states in argon were not found. Therefore, an analytical model developed by Drawin (Ref. 8) was employed in calculating the cross section of electron impact excitation, $Q_{EXC}(E)$ from lower state 1 to upper state u. The formula for this model is expressed as

$$Q_{UL}(E) = 4\pi a_0^2 \left(\frac{E_{H+}}{E_{UL}}\right)^2 f_{UL} B_1 \frac{\left(\frac{E}{E_u} - 1\right)}{\left(\frac{E}{E_u}\right)^2} \ln\left(1.25 B_2 \frac{E}{E_u}\right) \quad (7)$$

where a_0 is the Bohr radius, E_{H+} is the ionization energy of hydrogen, f_{UL} is the absorption oscillator strength, B_1. and B_2. are adjustable constants of order unity (Ref. 9:27). B_1. and B_2. were determined using partial argon cross-section data from Petersen and Allen (Ref. 10:6068),

12

Table I

Maximum Values of Low-Energy Electron Impact Excitation
Cross Sections for Selected Transitions in Argon*

Level	E_{TH} (eV)	E_{MAX} (eV)	Q_{MAX} (10^{-19} cm^2)
$7S_{3/2}°$	15.17	(58)**	(79.7)**
$4D_{1/2}°$	14.71	(58)**	(78.2)**
$4P'_{1/2}$	13.32	24	57.1
$4P'_{3/2}$	13.29	21	84.4
$4P_{1/2}$	13.27	20.6	46.7
$4P_{3/2}$	13.16	22.5	129.8
$4P_{3/2}$	13.15	21	78.0
$4P_{5/2}$	13.07	22	136

* (Ref. 4:291)

** Calculated using Drawin's formula (Ref 8)

13

Table II

Maximum Values of Low-Energy Electron Impact Excitation
Cross Sections for Selected Transitions in Cesium*

Level	E_{TH} (eV)	E_{MAX} (eV)	Q_{MAX} (10^{-16} cm^2)
$9D_{3/2}$	3.8	4.25	4.0
$9S_{1/2}$	3.5	4.0	7.6
$9S_{1/2}$	3.5	4.25	15.3
$7D_{3/2}$	3.0	4.0	19.5
$7D_{5/2}$	3.2	4.0	34.0
$8S_{1/2}$	3.0	3.5	19.0
$8S_{1/2}$	3.0	3.6	39.0

*   (Ref. 7:504)

14

and argon oscillator strength data from Wiese, et al. (Ref. 11:192). This analysis yielded excitation cross section data for the ground state ($3P_6$) to $4D_{1/2}°$ and $7S_{3/2}°$ transitions. These values are expressed parenthetically in Table I.

Modeling the excitation cross-section as a positive ramp function, we approximate $Q_{EXC}(E)$ as

$$Q_{EXC}(E) \approx M(E - E_{TH})$$ (8)

where E_{TH} is the threshold energy and M is the slope, given by

$$M = \frac{Q_{MAX}}{E_{MAX} - E_{TH}}$$ (9)

Therefore

$$Q(E) = Q_{MAX}\left(\frac{E - E_{TH}}{E_{MAX} - E_{TH}}\right)$$ (10)

If we assume a Maxwellian distribution of electron energies and if we rewrite the integral in Equation (6) in terms of the electron energy, we obtain

$$\langle R_{EXC} \rangle = \frac{2}{\sqrt{\pi}}\left(\frac{1}{kT_E}\right)^{\frac{3}{2}} \int_0^\infty R_{EXC} E^{\frac{1}{2}} e^{-E/kT_E} dE$$ (11)

For $T_E < E_{TH}$, the major contribution to the integral occurs in a limited energy range near the excitation threshold. Under these conditions, the integral may be reduced to an analytic form. This analysis, carried out in Appendix A, enables Equation (11) to be rewritten as

15

$$\langle R_{EXC} \rangle = 2\sqrt{\frac{kT_E}{\pi}}\, E_{TH}^{\frac{1}{2}}\, e^{-E_{TH}/kT_E}\, \left.\frac{\partial R_{EXC}}{\partial E}\right|_{E=E_{TH}} \tag{12}$$

Using Equation (9), and knowing that $v=(2E/m)^{1/2}$,

$$R_{EXC} = Q_{MAX}\left(\frac{E-E_{TH}}{E_{MAX}-E_{TH}}\right)\sqrt{\frac{2E}{m}}$$

$$\left.\frac{\partial R_{EXC}}{\partial E}\right|_{E=E_{TH}} = \frac{Q_{MAX}}{E_{MAX}-E_{TH}}\sqrt{\frac{2E_{TH}}{m}} = \sqrt{\frac{2}{m}}\,Q_{MAX}\,\frac{E_{TH}^{\frac{1}{2}}}{E_{MAX}-E_{TH}} \tag{13}$$

Now when Equation (13) is substituted back into Equation (12), the expression for $\langle R_{EXC}\rangle$ becomes

$$\langle R_{EXC}\rangle = \sqrt{\frac{8kT_E}{m\pi}}\, e^{-E_{TH}/kT_E}\, Q_{MAX}\left(\frac{E_{TH}}{E_{MAX}-E_{TH}}\right) \tag{14}$$

In the analysis of Equation (11) in Appendix A, it was assumed that $kT_E \ll E_{TH}$. At this point, we must consider whether or not this was true for the observed gas constituents. This assumption may be verified by numerically integrating Equation (11) and comparing the results to Equation (14). Such an analysis was performed (Ref. 12) for $T_E = 1$ eV and $E_{TH} = 2$ eV. For these conditions, similar to cesium, the numerical integration and the analytic form agree to within 60%. If $T_E = 1$ eV and $E_{TH} = 10$ eV, conditions similar to argon, the agreement is better than 80%. Hence, the approximation inherent in Equation (14) is considered acceptable.

Radiative Recombination Losses. The capture of a free electron into a bound atomic state is another means of populating the upper state. This process may be represented

16

for atomic species B as $B^+ + e^- -> B^* + hf$, where f is the frequency of the resultant photon. In Equation (5) the rate of this interaction is represented as $\langle R_{REC} \rangle n_E$. A typical interaction cross section is on the order of 10^{-19} cm² (Ref. 13). Hence, for an electron with a velocity of 10^7 cm/sec, and for an electron number density on the order of 10^9/cm³, we find that $\langle R_{REC} \rangle n_E$ is approximately 10^{-3}/sec. It will be seen in the next section that this process is negligible.

Radiative Losses. In Equation (5), it is seen that a mechanism by which an excited state is depopulated is by radiative decay to lower lying states. Consider the 8S state in cesium shown in Figure 4. Obeying the selection rules, a radiative transition from this state is allowed to the $7P_{3/2}$, $7P_{1/2}$, $6P_{3/2}$, and $6P_{1/2}$ states. If the A coefficients are A_1, A_2, A_3, and A_4, respectively, then the total loss to the 8S state may be expressed as $(A_1 + A_2 + A_3 + A_4)N_U$. Where N_U is the population of the uppermost lying state, which in this case is 8S. This is a fairly simple expression for a state such as 8S, but the number of terms that need to be included increases as one considers states of higher n values. In general, the rate of loss to various lower states l is expressed as $N_U \sum_l A_{UL}$.

Tables III and IV list the radiative loss term, $\sum A_{UL}$, for each of the observed transitions in argon and cesium. The values for A_{UL} for argon were obtained from Weise, et al (Ref. 11:192), with uncertainties ranging from 25% to 50%. The listed values for A_{UL} for cesium were calculated
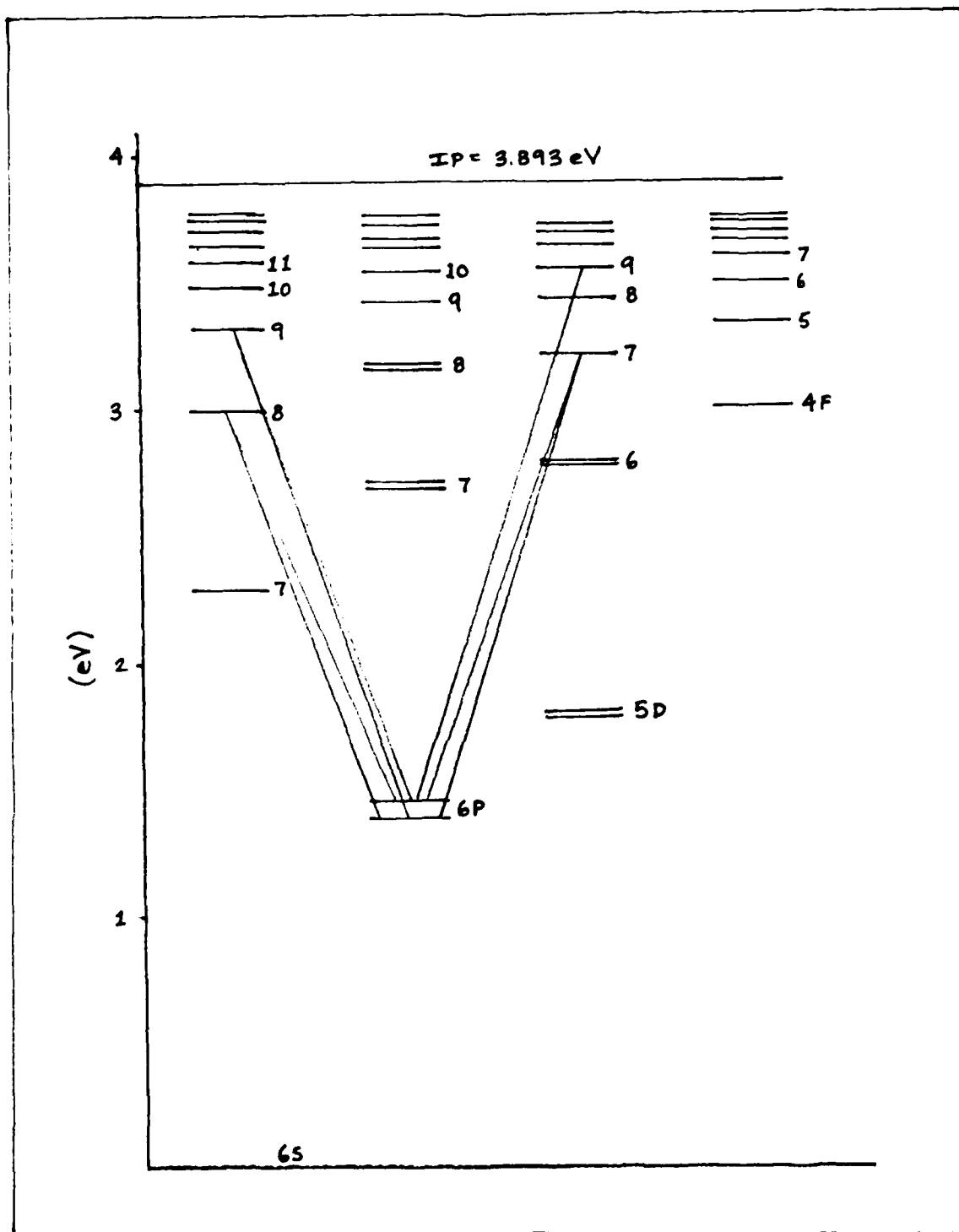
17

FIG. 4: Energy level diagram for Cs I. Transitions observed in this experiment have been sketched in.

from oscillator strength data collected by Fabry and
Cussenot (Ref. 14:836), but no estimate of the uncertainty
is given. However, Stone (Ref. 15:1151) calculated the same
quantity for cesium and estimated the error to be within
50%. From Table III, the radiative losses for argon are
seen to be on the order of 10^7/sec. In Equation (5), this
term appears in the denominator along with the radiative
recombination term, which was earlier found to be on the
order of 10^{-3}/sec. Clearly, radiative recombination
processes are negligible.

Electron Impact De-excitation Losses. Another process
of depopulating an excited state is by electron impact de-
excitation, denoted in Equation (5) by $<R_{DEXC}>n_E$. A
general result of detailed balance is that the cross section
of de-excitation, Q_{DEXC} , may be expressed in terms of the
cross section, Q_{EXC} , of the reverse process:

$$Q_{DEXC}(E) = \frac{(E+E_u-E_L)\ Q_{EXC}\ (E+E_u-E_L)}{E} \qquad (15)$$

where E is the electron energy, and E_u and E_L are the
levels of any two states in the atom. But for our purposes
here, due to the large population of the ground state
relative to any excited state, we assume that most
collisions will excite from the ground state, therefore
E_L =0. Using the data in Table I and assuming a 1 eV
electron, A typical value for Q_{DEXC} (E) is 10^{-17}cm^2. A
similar analysis for cesium produces a value of 10^{-13} cm^2.
With the electron velocity V on the order of 5×10^7 cm/sec

19

Table III

Relative Transition Probabilities and Radiative
Loss Terms for Selected Transitions in Argon*

TRANSITION	λ (Å)	$A(10^8/sec)$	$\Sigma A(10^8/sec)$
$4P_{5/2} \rightarrow 7S_{3/2}^{\circ}$	5928.8	0.011	0.052
$4P_{1/2} \rightarrow 4D_{1/2}^{\circ}$	6871.3	0.0290	0.116
$4S_{3/2}^{\circ} \rightarrow 4P'_{1/2}$	6965.4	0.067	0.857
$4S_{3/2}^{\circ} \rightarrow 4P'_{3/2}$	7067.2	0.0395	0.720
$4S_{3/2}^{\circ} \rightarrow 4P'_{3/2}$	7384.0	0.087	0.720
$4S_{3/2}^{\circ} \rightarrow 4P_{1/2}$	7514.7	0.430	0.716
$4S_{3/2}^{\circ} \rightarrow 4P_{3/2}$	7635.1	0.274	0.753
$4S_{3/2}^{\circ} \rightarrow 4P_{3/2}$	8006.2	0.0468	0.753
$4S_{3/2}^{\circ} \rightarrow 4P_{3/2}$	8103.7	0.277	0.753
$4S_{3/2}^{\circ} \rightarrow 4P_{5/2}$	8115.3	0.366	0.478

*(Ref. 11:192)

Table IV

Relative Transition Probabilities and Radiative
Loss Terms for Selected Transitions in Cesium[*]

TRANSITION	λ (Å)	$A(10^8/\text{sec})$	$\Sigma\, A(10^8/\text{sec})$
$6P_{1/2} \rightarrow 9D_{3/2}$	5664.0	0.0226	0.0644
$6P_{1/2} \rightarrow 9S_{1/2}$	6354.6	0.0103	0.0550
$6P_{3/2} \rightarrow 9S_{1/2}$	6586.5	0.0181	0.0550
$6P_{1/2} \rightarrow 7D_{3/2}$	6723.3	0.0711	0.1124
$6P_{3/2} \rightarrow 7D_{5/2}$	6973.3	0.1957	0.2265
$6P_{1/2} \rightarrow 8S_{1/2}$	7608.9	0.0214	0.0997
$6P_{3/2} \rightarrow 8S_{1/2}$	7943.9	0.0385	0.0997

[*](Refs. 14:836, 15:1151)

and an electron number density n_E of $10^9/cm^3$, then the term $\langle R_{DEXC} \rangle n_E$ is approximately $10^{-1}/sec$ for argon and $10/sec$ for cesium. But this competes with radiative losses, which were found earlier to be on the order of $10^7/sec$. Hence, electron impact de-excitation is safely ignored for both argon and cesium.

Quenching Losses. If the excited atom collides with a neutral particle, the electronic energy may be "quenched" when it is transferred into the kinetic or electronic energy of the neutral. Consider the following quenching interactions in an argon/cesium low pressure plasma:

$$Ar + Ar \rightleftharpoons Ar + Ar^* \tag{16a}$$

$$Cs + Cs \rightleftharpoons Cs + Cs^* \tag{16b}$$

$$Ar^* + (Ar \text{ or } Cs) \rightleftharpoons Ar + (Ar \text{ or } Cs) \tag{16c}$$

$$Cs^* + (Ar \text{ or } Cs) \rightleftharpoons Cs + (Ar \text{ or } Cs) \tag{16d}$$

$$Ar^* + Cs \rightleftharpoons Ar + Cs^+ + e^- \tag{16e}$$
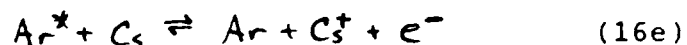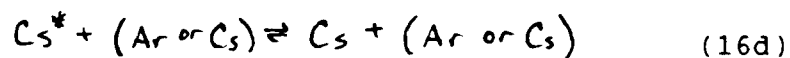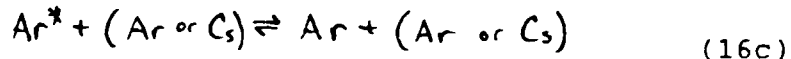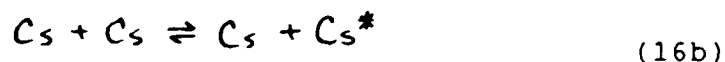
The first two processes are of little interest because they do not change the net composition of the plasma. The second two processes are true quenching interactions in which the colliding neutral particle gains kinetic energy. The last process, commonly called Penning ionization, also serves to deplete the excited state population of argon. There is not an analogous interaction which describes ionization or excitation of argon by cesium for the simple reason that

22

argon excited states lie at ~13 eV, while excited cesium states do not exceed 3.9 eV.

These processes are represented in Equation (5) by $\langle R_0 \rangle n_0$, or by $\langle QV_0 \rangle$. V_0 is the velocity of the neutral and, strictly speaking, Q should be the cross section for those atom-ion collisions which results in one of the above listed interactions. Making the hard sphere approximation, and assuming that 100% of excited atom collisions with neutrals result in quenching, Q may be estimated to be to be on the order of 10^{-15} cm^2 and at a gas temperature of 500 K, the neutral particle velocity will be 5 x 10^4 cm/sec. At operating pressures of 1.0 Torr argon and 0.04 Torr cesium, the number density of neutral argon is 3 x 10^{16}/cm^3, and for neutral cesium it is 10^{15}/cm^3. For the processes indicated in equations (16c) and (16d), $\langle R_0 \rangle n_0$ is about 10^5/sec, and for the Penning ionization interaction, $\langle R_0 \rangle n_0$ is about 10^4/sec. However, both of these are small in comparison to the rate of radiative loss which is on the order of 10^7/sec. Hence, quenching effects are ignored. This is a useful simplification for most transitions. However, one will note that several transitions in argon have radiative loss terms which are as low as 10^5/sec. In these situations, quenching effects may play a role. But this analysis does not take this into account.

23

The Resultant Expression

We have considered each term in Equation (5) and have found that electron impact excitation and radiative de-excitations are the dominant processes within a low pressure argon/cesium plasma. In comparison to these processes, radiative recombination, electron impact de-excitation and quenching losses were found to be small enough to ignore. Therefore, Equation (5) may be written as

$$I_{uL} = \frac{A_{uL}(E_u - E_L) \langle R_{exc} \rangle n_0 n_E}{\sum_L A_{uL}}$$ (17)

We substitute for $\langle R_{exc} \rangle$ from Equation (14), and knowing that $E_u - E_L = hc/\lambda_{uL}$, we may re-express Equation (17) as

$$G(E) \equiv \ln \left\{ \frac{I_{uL} \lambda_{uL} \sum_L A_{uL}}{A_{uL} C} \right\} = \frac{-E_u}{kT_E} + B(n_E, T_E)$$ (18)

where

$$C = \frac{Q_{MAX}(E_{MAX} - E_{TH})}{E_{TH}}$$ (19)

and

$$B(n_E, T_E) = \ln \left\{ hc \sqrt{\frac{8kT_E}{m\pi}} n_0 n_E \right\}$$ (20)

At a given spatial location within the discharge n_E and T_E will be constant, thereby rendering $B(n_E, T_E)$ constant as well. This enables Equation (18) to be viewed as a linear equation in which the slope of E_u vs. $G(E)$ will be inversely proportional to the electron temperature. These are the equations upon which the results of this study are based.

24

III. Experimental Apparatus

The apparatus described in this chapter enables spectral intensity of an argon/cesium discharge to be measured. This apparatus can be divided into several distinct subsystems: the diode, the spectroscopic, the data collection, and the vacuum and heating systems. Each of these is described below.

The Diode System

The Diode Structure. The heart of the experimental apparatus is the two molybdenum electrodes suspended in the center of a five-way stainless steel cross, as depicted in Figure 5. The electrodes are 2.54 cm diameter disks with a 1.8 cm gap.

Three arms of the five-way cross terminate in a conflat-type flange mounted sapphire window. Spectroscopic measurements are taken through one of these windows, visual observations are made through another, and the third window allows future experimenters to direct a laser beam into the discharge region. The electrodes are suspended through a glass-metal seal installed at the top of the fourth stainless steel arm. The fifth arm gives the discharge region access to the reservoir of cesium and to the vacuum/gas handling system. A stainless steel nipple, 7.6 cm in length and 1.9 cm outer diameter, serves as a reservoir for the cesium. The reservoir was located 14 cm from the discharge region.

25

A. Conflat-type sapphire windows

B. Electrode leads and glass-metal seal

C. Cesium Reservoir

D. Inoperative Baratron

FIG. 5: Diode System

26

A tubular quartz shield, 6.0 cm outer diameter, is placed around the electrodes to prevent the discharge from striking between the back side of the cathode and the nearby wall of stainless steel. The shield is perforated with three 3.2 cm holes. This gives the cesium vapor freedom to diffuse into the discharge region and permits spectroscopic and visual observations to be made without having to look through what would effectively be a poor quality quartz lens.

The electrodes are connected in series with a 10 KΩ resistor, a Simpson 270 multimeter acting as an ammeter, and a Keithley constant voltage power supply. A Triplett 630-PLK multimeter, acting as a voltmeter, is installed in parallel with the electrodes.

Discharge Behavior. Visually, the discharge appeared as shown in Figure 6, where each of the labeled regions are described below. Aston's dark space, (A), was approximately 0.1 cm in width. The cathode glow, (B), was a bright lavender and was less than 0.1 cm wide. The non-equilibrium character of the discharge in these regions leads to a violation of the assumption that the plasma is in a "quasi-neutral" state. The characteristic length, L, is a measure of the distance over which quasi-neutrality is not maintained. We know that

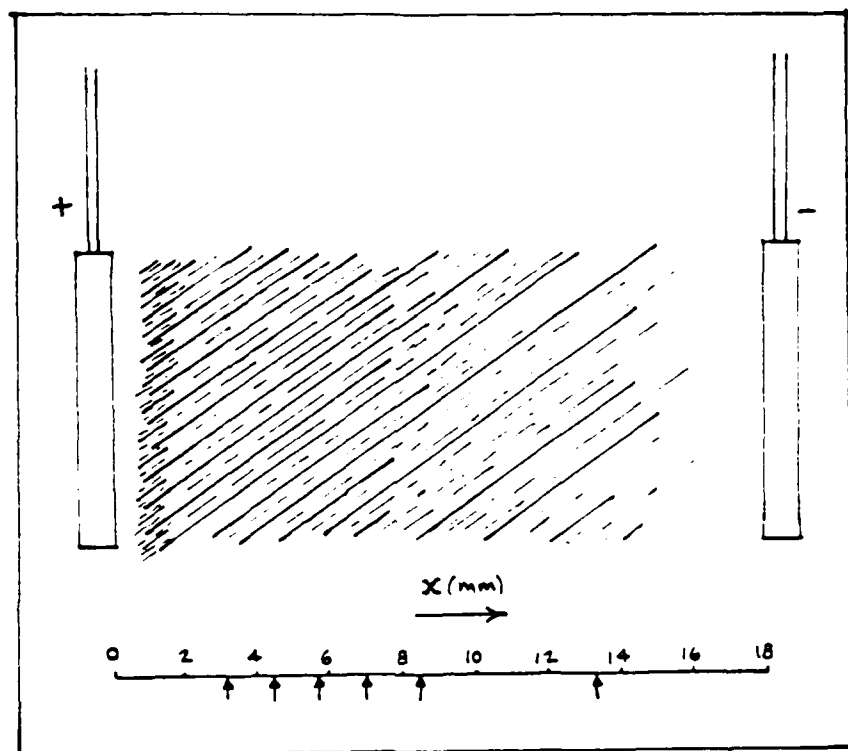$$L = \sqrt{\frac{kT_E}{4\pi n_e e^2}} \tag{21}$$

27

FIG. 6: Schematic diagram of visual appearance of argon/cesium discharge operating at 0.9 Torr argon, 0.04 Torr cesium, and a current density of 1.05 mA/cm^2. Arrows point to locations in discharge which were spectroscopically observed.

where T_E is in eV, n_E is in cm^{-3}, and L is in cm. For a cathode fall voltage of 170 volts and an electron number density of 10^9/cm^{-3}, we find that L=0.3 cm. This is very close to the dimensions of regions A and B in Figure 6.

The negative glow, (C), appeared to continuously merge with the cathode glow, hence the cathode dark space was not observed. The negative glow began as a bright lavender at the boundary with the cathode glow. It gradually faded to a dim purple 1.2-1.5 cm from this boundary. This dimension compares well with the expected length of 1.0 cm, as discussed in Chapter I.

The Spectroscopic System

The purpose of the spectroscopic system was to isolate a particular region of the plasma, image the optical radiation from that region onto a spectrometer, and convert the optical signal into an electrical signal. The arrangement of components necessary to fulfill this task is shown in Figure 7.

The radiation generated by the discharge passes through the hole in the quartz tube and then encounters the sapphire window, which has at least 80% transmission in the wavelength region 250-5500 nm. Upon leaving the diode system, the radiation passes through the first of two slits. The pair of slits, the first with a width of 0.2 cm and the second with a width of 0.5 cm, are mounted on a single micrometer-driven translatable stage, which can be moved so as to optically isolate a particular slice of the plasma.

29

FIG. 7: Spectroscopic System

A. Molybdenum electrodes
B. Tubular quartz shield
C. Sapphire window
D. Pair of translatable slits
E. Translatable lens
F. Beam chopper

G. 0.5 m spectrometer
H. Photomultiplier tube
I. Lock-in amplifier
J. Digital voltmeter
K. GPIB interface
L. Micro-computer
M. Floppy disk
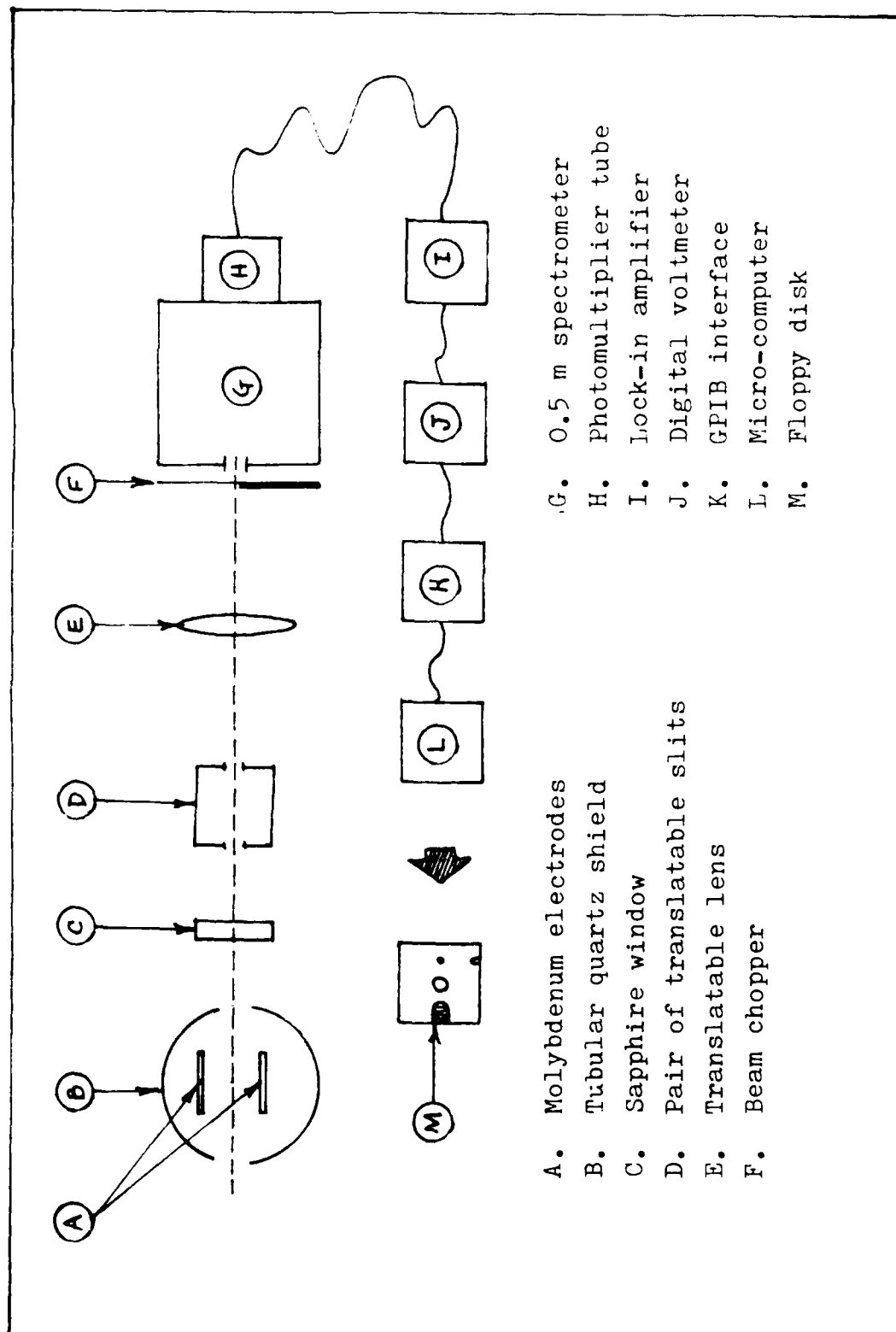
All of the radiation which passes through the slit then falls onto a separately translatable, 10 cm focal length, 7.62 cm diameter lens. The lens is positioned to ensure that the radiation which passes through the slits is imaged onto the entrance slit of the spectrometer (0.5 mm slit widths). Knowing the widths of each slit and the magnification of the optical system, it is determined that the typical width of any observed slice of the plasma was 0.5 mm.

Before entering the spectrometer, the radiation encounters a beam chopper with a 50% duty cycle. This chopper provides a synchronizing signal to the lock-in amplifier described below. The 0.5 m Spex 1870 spectrometer, driven by a Spex CD2 Compudrive, selects the desired wavelength and images it on the Hammamatsu R763 photomultiplier tube.

The PMT output is routed to a lock-in amplifier (10MΩ input impedance, EG&G Model 117) which converts the PMT current to a voltage signal. The output of the amplifier is detected and digitized by a Hewlitt-Packard 3457A digital voltmeter. A parallel GPIB interface (Seitz 6450A) then routes the DVM signal to an HP 9836 micro-computer system, where it is recorded onto a floppy disk. Alternatively, the analog data can also be recorded onto an HP 7132A strip recorder.

Because we have chosen the spectral line intensity method of measuring the electron temperature, it is not

31

necessary to measure absolute intensities or to use high spectral resolution. This leads to significant experimental simplification in the sense that, although the optics are carefully aligned, high precision is not necessary.

The Vacuum System

The vacuum system depicted in Figure 8 consists of a small Welch roughing pump and a Varian model 0159 2-inch air cooled diffusion pump. It is capable of evacuating the diode to pressures of 10^{-6} Torr. Initially, pressures were measured using a baratron attached to the diode structure. But this baratron failed at the high operating temperatures of the diode system. After this failure, an MKS model 77 differential baratron was installed as shown in Figure 8. This enables the argon pressure to be measured at room temperature prior to being introduced into the diode. An ion gauge and Granville Phillips 260 gauge controller serves to measure the pressure of the empty cell.

The Heating System

The stainless steel structure is heated with six 4-foot long heat tapes. The tapes are serially connected to one another in three sets of two. These three sets are also connected in parallel with one another to an HP 6443B power supply. An insulating jacket of aluminum-oxide fiber is wrapped around the entire structure. The cesium reservoir is heated with a separate heat tape, controlled by a Variac auto transformer. The reservoir is not wrapped with

32
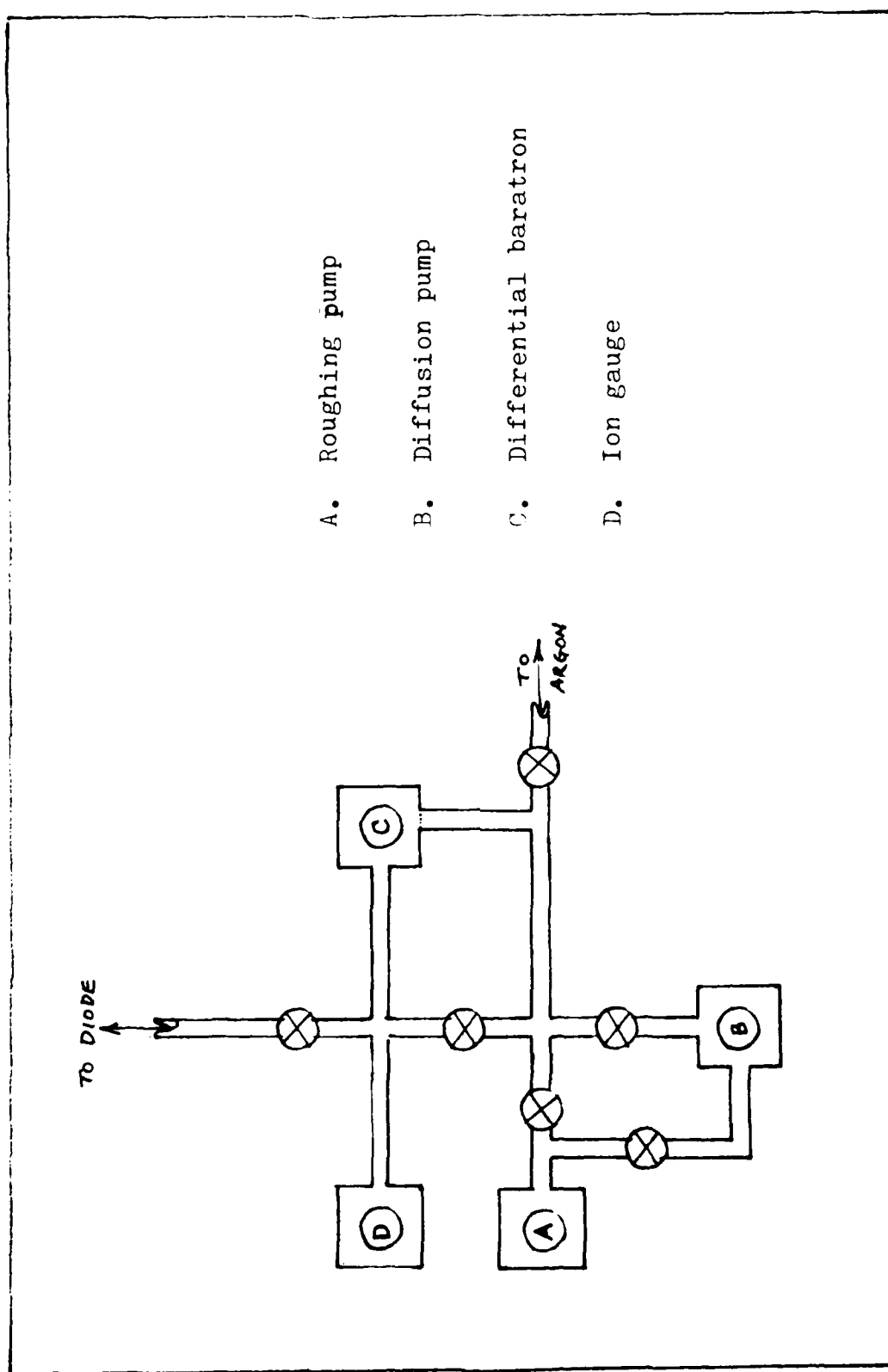
A. Roughing pump

B. Diffusion pump

C. Differential baratron

D. Ion gauge

TO DIODE

TO ARGON

FIG. 8: Vacuum System

33

aluminum oxide, which allows for rapid cooling.

Temperatures are monitered in three different locations. One K-type bead probe (Chromel-Alumel) is placed at the junction of the sapphire window and the stainless steel flange. The seal around this window has an upper temperature limit of 250°C. By monitering the temperature at this location, we ensure that the seal does not overheat. We also ensure that this temperature remains well above that of the reservoir in order to prevent cesium from condensing onto the window.

A similar probe is located at the glass-metal seal where the electrode leads enter the cell. Due to the shape of this seal, portions of the glass are exposed to the air, despite the aluminum-oxide wrap. Hence, this is the coolest temperature of the entire cell. But since this temperature is kept well above the temperature of the reservoir, the cesium vapor in the system does not condense on this relatively cool portion of the cell.

A K-Type junction probe lies between the stainless steel exterior of the cesium reservoir and the heat tape. The temperatures measured here are assumed to be the temperature of the cesium inside the reservoir. The vapor pressure at this temperature is then obtained by means of a vapor pressure curve for cesium (Ref. 16:475). As with the other two probes, measurements are taken with a Fluke digital multimeter equipped with a linearization module.

IV. Experimental Procedure

Using the equipment described in the previous section, the spectral intensities of the plasma are measured with the procedure detailed below. This procedure is presented in three stages: the preliminary processes needed to "break-in" the new system, calibrating the spectroscopic system, and the spectral measurements themselves.

Breaking the System In

Prior to obtaining the spectral measurements, it was necessary to perform a variety of preliminary procedures. First, after wrapping the entire cell in heat tapes and aluminum-oxide blanket, it was necessary to wait for the apparatus to come to a thermal equilibrium with its surroundings. The thirty pounds of stainless steel provided enough thermal "inertia" to make the process of stabilizing at 250°C a two-day process. When a stable temperature was achieved, the cell was then left at 250°C under a vacuum of 10^{-6} Torr for several more days to allow the impurities to be "baked-out" of the system.

Additionally, over a span of a few weeks, the operating voltage dropped steadily. It eventually stabilized at about 130 volts, at which point it was assumed that the system had been "broken-in" and that we could proceed with the measurements.

Calibration of Spectrometer

The spectrometer was calibrated using a Photon Technol-

35

ogies, NBS traceable calibration lamp. The spectral

response of the spectroscopic system to this source was then

compared to the known blackbody calibration spectrum,

provided by the lamp's manufacturer, over the wavelength

range of 320-820 nm. The ratio of the blackbody intensity

to the measured intensity provided a calibration factor for

any wavelength within this range.

The resulting calibration curve, which was normalized

at 600 nm, is shown in Figure 9. The sharp peak at 680 nm

is due to a sharp drop in the spectral response of the

spectrometer. It was thought that this effect was an effect

of the grating blazing, commonly called a Wood's anomaly

However, in discussions with the manufacturer, it was found

that the grating used in this experiment is blazed for a

maximum response at 700 nm.

Although this spike is not understood, it is believed

to be a real effect of the spectrometer. If this were not

the case, then the calibrated intensities of those spectral

lines which fall between 660-710 nm would be expected to

deviate substantially from those lines which are in the

flatter portions of the spectral response. However, no such

deviation is observed.

Spectral Measurements

The spectral measurements began once the above proce-

dures had been carried out. The process of taking these

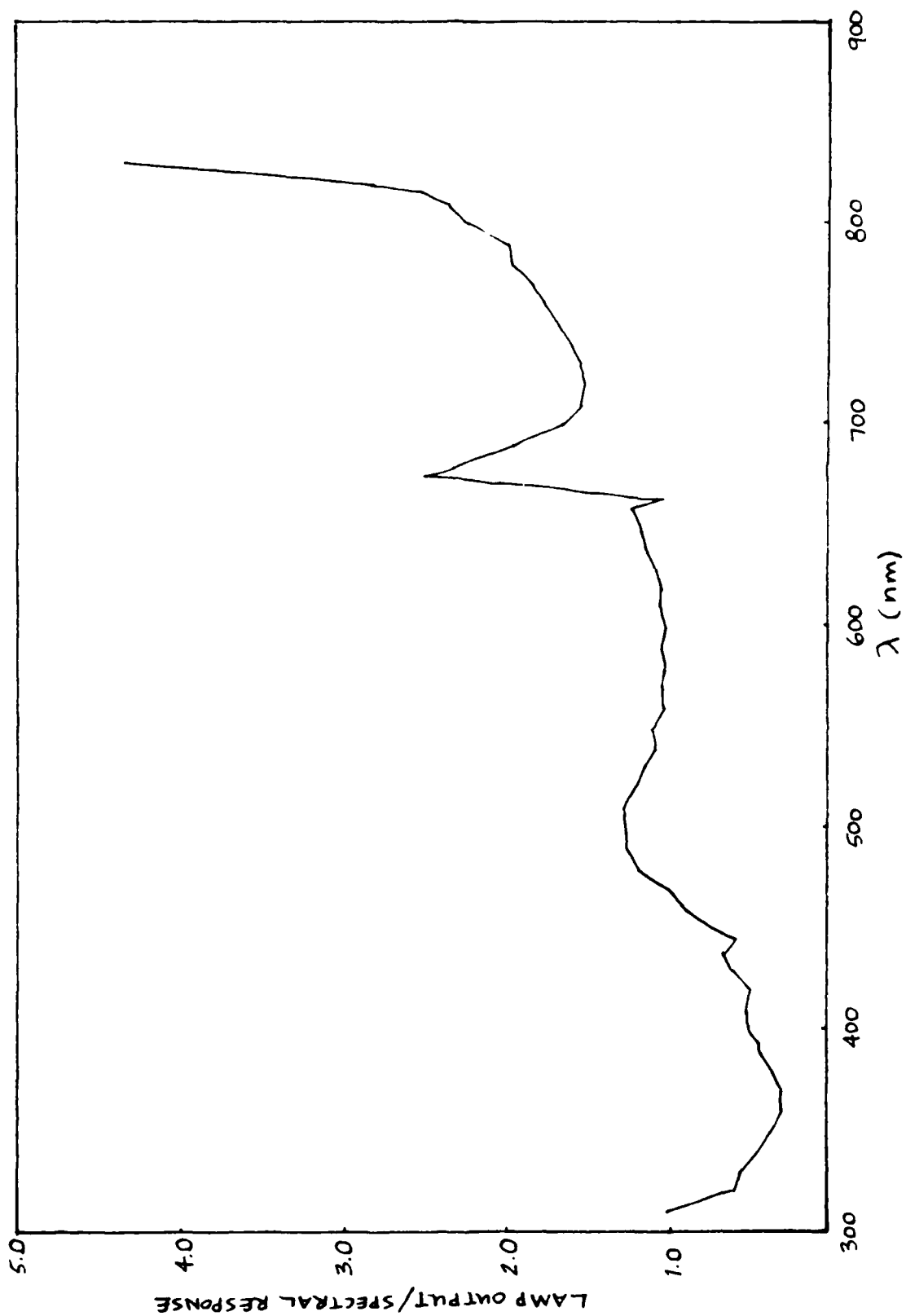measurements can be broken down into the following steps:

36

FIG. 9: Normalized calibration curve for the spectroscopic system. The vertical axis is the ratio of the blackbody intensity of the calibration lamp to the measured spectral response.

37

(1) Position the double slits at the desired spatial location. This study observed the discharge at 3.18, 4.45, 5.72, 6.99, 8.26, and 13.34 mm from the cathode.

(2) Using the spectrometer driver, slew the spectrometer to the wavelength of a bright spectral line. Observing the amplifier response, adjust the position of the lens until the response is maximized. When this occurs, it is assumed that the image of the discharge region has been centered on the spectrometer entrance slit.

(3) Record the current, the amplifier scale, and the width of the spectrometer slits. The data presented here was taken within one twelve hour period, but during that time the current drifted in the region of 4.7-5.9 mA. Both the entrance and exit slits of the spectrometer were set at 0.5 mm.

(4) Scan the spectrometer over the region of interest. Typically, these scans were taken over wavelength regions of 100 nm or less and were intended only to capture those spectral lines which were of particular interest. Hindsight suggests that a more thorough method would inlude the entire wavlength region 400-820 nm in one scan. This would facilitate both the data collection and data

38

analysis processes. However, in taking longer
scans, one would sacrifice the ability to optimize
the scanning speed and amplifier response for a
small wavelength region.

(5) Store the data on floppy disk. Using a software
package originally designed by Dr. Charles
deJoseph and subsequently modified by Lieutenant
James Shoemaker, both of the Air Force Wright
Aeronautical Laboratories, the spectrometer scans
and data collection were fully automated. This
same software proved useful in the data analysis
described in the next chapter.

Determining Which Transitions to Observe

Before taking the spectral scans, it was important to
ascertain which lines were of most importance. By identify-
ing thes. particular lines, we could ensure that the data
would be sufficient to measure the electron temperature.
The selection of lines depended on the criterion described
below.

(1) The sensitivity of the photomultiplier tube
limited the observations to those lines in the region
of 300-820 nm.

(2) Spatial resolution of the electron temperature
demanded that the chosen lines be observable throughout
the length of the discharge region.

(3) Radiative trapping eliminated some lines from
being selected. The process of radiative trapping
implies that every photon produced by spontaneous
emission is reabsorbed before it leaves the plasma.
For example, the 6S-nP series in cesium were
indistinguishable from the noise even though these
should have been among the strongest lines in the
spectrum. This was attributed to radiative trapping.

(4) An observed line must not overlap a neighboring
line to the extent that they become indistinguishable
from one another.

(5) In order to obtain data over a range of energies,
it was helpful to choose a complete series of transi-
tions. In cesium, the 6P-nD and 6P-nS series were
observed. Due to an oversight by this experimenter, a
similar series in argon was not selected, even though
an abundance of argon lines lie in the 300-500 nm
range. This error resulted in a large gap in the range
of energies covered by the argon spectral data.

(6) A result which is clearly evident in the cesium
emission spectra is the significant enhancement of the
intensity of the $6P_{1/2} \rightarrow 10D_{3/2}$ transition (λ =546.6
nm). One would have expected this transition to be
much less intense than the $6P_{1/2} \rightarrow 9D_{3/2}$ (λ =566.4
nm) transition because of the larger value of n. But

40

as shown in Figure 10, such is not the case. A similar

effect is also suspected for the $6P_{1/2} \rightarrow 11S_{1/2}$

transition. Those lines which were thus enhanced were

not used in the spectral analysis.

The transitions which were chosen on the basis of these

criteria are listed in Tables III and IV. Hereafter, this

set of transitions will be referred to as the "transitions
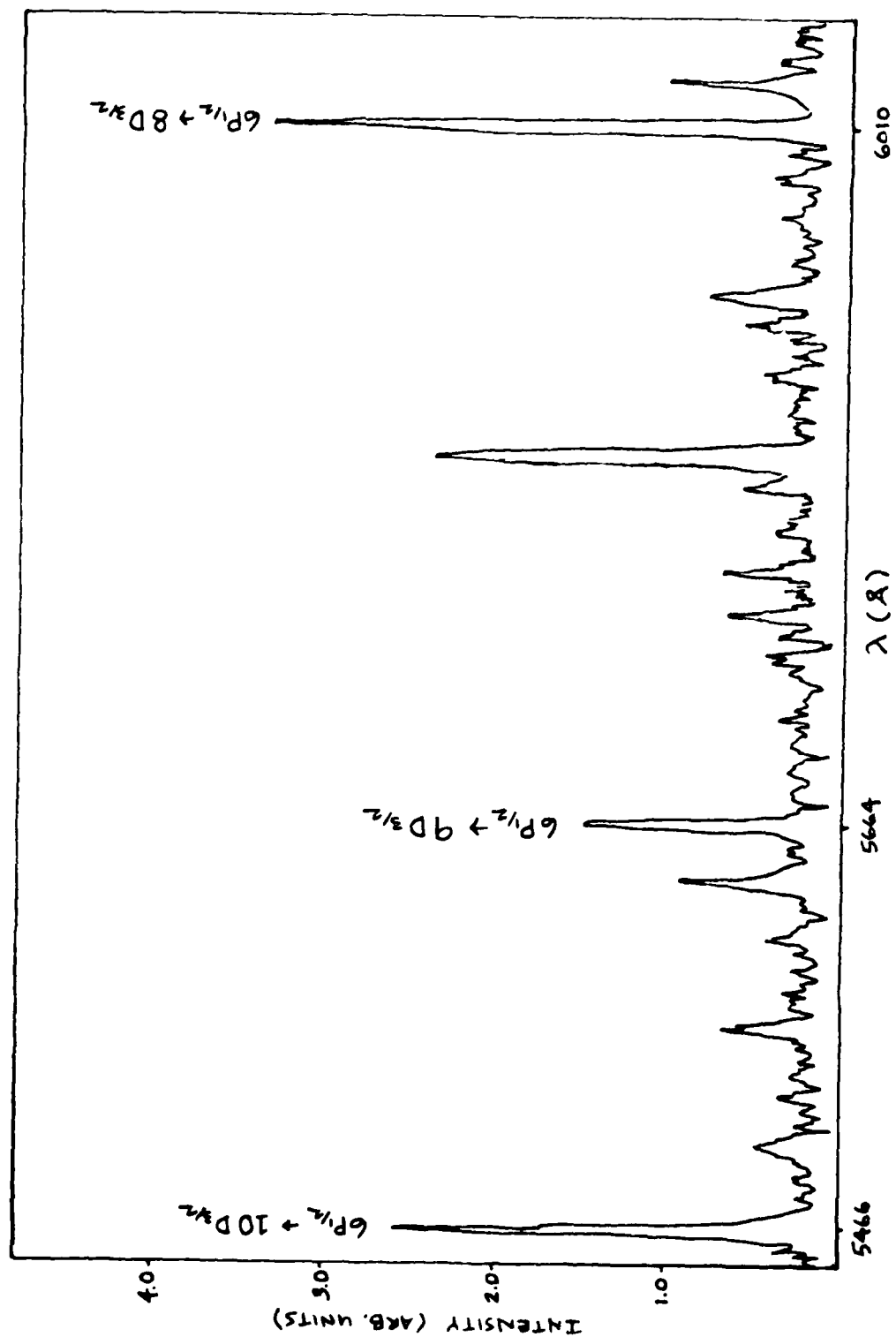
of interest" or "spectral lines of interest."

FIG. 10: Enhancement of the 6P(1/2) → 10D(3/2) transition. Due to this unexplained enhancement, this transition was not used in the spectral analysis of this study.

42

VI. Data Analysis and Results

The above procedure garnered a set of several spectral scans at each of six spatial locations. At each of these locations, various portions of the emission spectrum from 545-815 nm were observed. Each of these scans included one or more spectral lines of interest in either argon or cesium. This raw data, of which an example appears in Figure 11, was reduced in order to yield a relative spectral intensity. Then using the equations derived in chapter II, these intensities were used to calculate the electron temperature of the plasma. This chapter explains each of these steps in the process of transforming the raw data into a measurement of electron temperature.

Calculating the Intensity

Taking a closer look at the data in Figure 11, we select one of the lines of interest and reproduce it in more detail in Figure 12. In order to calculate the full intensity of this line, we follow this procedure:

(1) Estimate the average level of the backround, H_B.

(2) Measure the height of the peak, H_P, and define the total height, H_T, as $H_T = H_B + H_P$.

(3) If $H_{1/2}$ is the half-maximum height of the peak as measured from the backround level, then

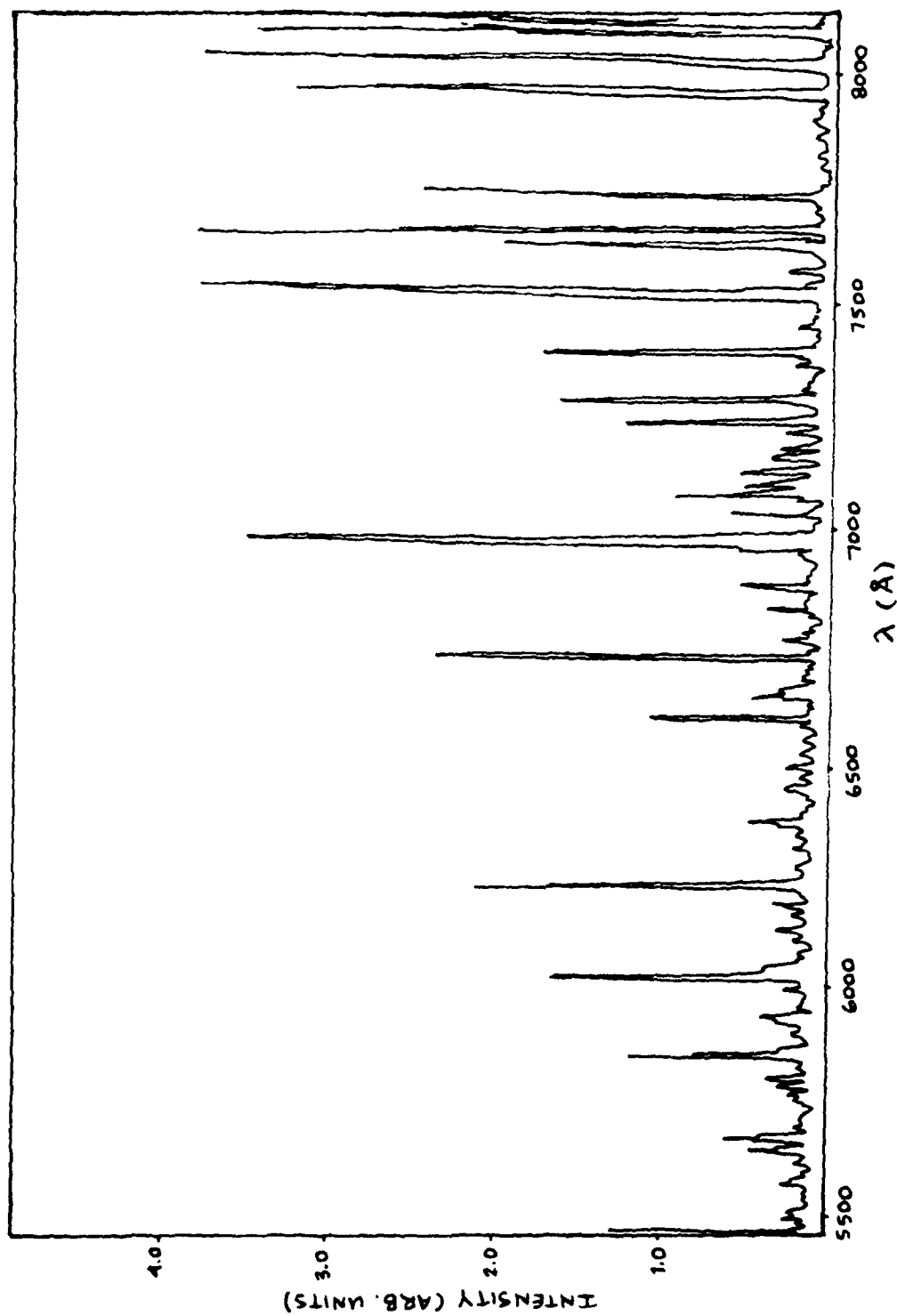$$H_{\frac{1}{2}} = (H_T - H_B) / 2$$

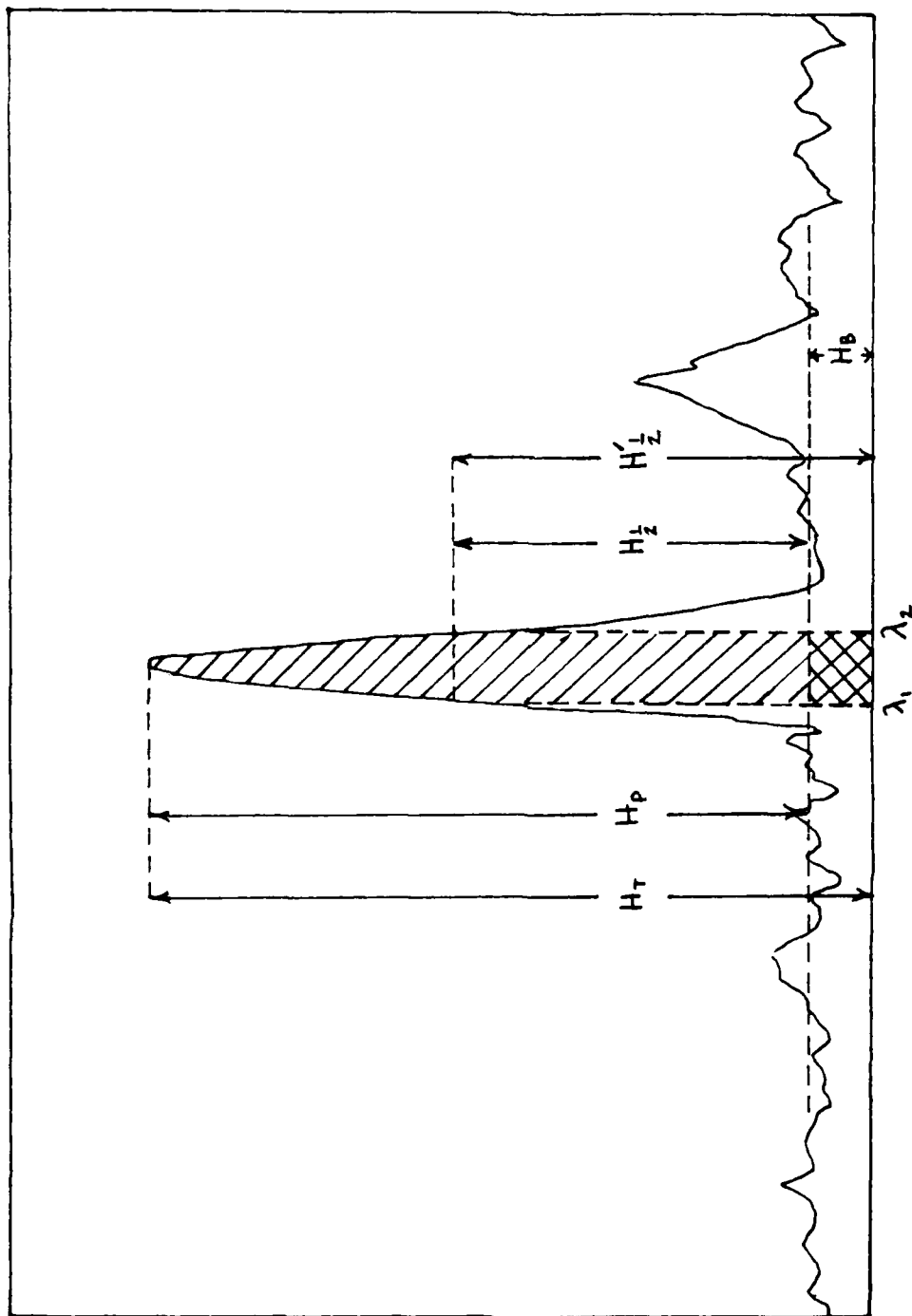43

FIG. 11: Sample spectral scan of 5450—8150 Å.

44

FIG. 12: Detail of how spectral intensities were measured

But the software gave intensity values as measured from the zero intensity level, without subtracting the backround. Hence, we define $H'_{1/2}$ to be the half-maximum height as measured from the zero intensity level, where $H'_{1/2} = H_{1/2} + H_b$. Therefore

$$H'_{\frac{1}{2}} = \frac{H_T + H_B}{2}$$

(4) By marking the locations of the half-maximum intensity, the corresponding values of λ_1 and λ_2 are obtained, where FWHM $= \lambda_2 - \lambda_1$.

(5) The software which is responsible for collecting the data also integrates the area under the entire spectral output. This yields a value for the integrated area, $A(\lambda)$, at any point in the spectrum. Hence, $A(\lambda_2) - A(\lambda_1)$ is the area of the shaded portion of the line profile in Figure 12.

(6) The backround area, which has been cross-hatched in Figure 12, is subtracted from the quantity $A(\lambda_2) - A(\lambda_1)$ in order to find the total area, $A_T(\lambda)$:

$$A_T(\lambda) = \left(A(\lambda_2) - A(\lambda_1) \right) - H_B \left(\lambda_2 - \lambda_1 \right)$$

(7) Before obtaining a final value for the integrated intensity, two more terms need to be evaluated. The calibration factor, $C(\lambda)$, is assumed to be constant in the wavelength region between λ_1 and λ_2. A value for $C(\lambda)$ is taken from Figure 9. The multiplier on the

lock-in amplifier also needs to be taken into account.
Denote this factor by W. Therefore, the integrated
intensity I is given by

$$I = \left(\left(A(\lambda_2) - A(\lambda_1) \right) - H_B(\lambda_2 - \lambda_1) \right) C(\lambda) W \qquad (22)$$

Calculations

Following the procedure outlined above, the integrated
intensity values, I, are calculated from the raw spectral
data. But this information needs to be processed through
Equation (18),

$$G(E) \equiv \ln \left\{ \frac{I_{UL} \, \lambda_{UL} \, \sum_L A_{UL}}{A_{UL} \, C} \right\} = \frac{-E_u}{kT_E} + B(\eta_E, T_E) \qquad (18)$$

before the electron temperature can be determined. The
values for A_{UL} and $\sum A_{UL}$ are taken from Tables III and IV.
The quantity C is defined in Equation (19) and is calcula-
ted from the data listed in Tables I and II. Knowing the
characteristic wavelength, λ_{UL}, of the transition, G(E) is
calculated for the spectral lines of interest in both argon
and cesium at six spatial locations within the discharge.

The results are presented in Appendix B in the plots of
G(E) vs E for both argon and cesium spectral emission data
at each spatial location. Using a least squares fitting
program, a linear fit is then applied to the data. This
produces a value for the slope and standard deviation of
the slope, where the slope is inversely proportional to
electron temperature.

One will note that no line has been plotted for the

47

argon emission data at 13.34 mm from the cathode. At this distance into the negative glow, argon emission intensities had dropped significantly. Therefore, at this spatial location the sample of lines was deemed as insufficient to determine a line. The data is only presented for the sake of completeness.

A prominent feature of these results is the large uncertainty in the calculated slope of G(E) vs. E, and hence in the uncertainty of the value for T_E . The uncertainty calculations reveal that the experimental uncertainty of 12% is dwarfed by the uncertainties in the literature values for oscillator strengths and transition probabilities, which vary from 25% to 60%. These large uncertainties in litera-ture values are the limiting factor in assessing the relia-bility of the measurements.

Another outstanding feature is that two electron temperatures are measured by observing the emission spectra of the two different gas species. The argon data measures an average electron temperature of 13,500 K throughout the entire discharge region, while the average temperature measured by the cesium data is 8200 K. This result is discussed in the following chapter.

VII. Conclusions and Recommendations

The purpose of this study was to apply spectral intensity measurements as a means to measure the electron temperature in a low pressure argon/cesium plasma. The device was operated at 0.9 Torr argon, 0.04 Torr cesium, and at a current density of $1.05mA/cm^2$. The electron temperature was determined spectroscopically using the line intensity technique outlined in Chapter II. This method was applied to the 6P-nS and 6P-nD series in cesium and to a set of transitions in argon. The cesium emission data characterize the low-energy electrons as an 8200 K Maxwellian, whereas the argon emission data a temperature of 13500 K. Within the uncertainties of the results, it is not possible to discern any spatial variation in these temperatures.

If the distribution of electron energies was purely Maxwellian, as assumed in the theoretical discussion of Chapter II, then one would have expected both argon and cesium data to reveal a single electron temperature. The fact that this study yields two distinct temperatures based on a measurement of the emission by the argon/cesium plasma confirms that under the given highly non-equilibrium plasma conditions, the electron energy distribution is non-Maxwellian.

Referring to the electron energy distributions sketched in Figure 2, we expected the negative glow to contain two groups of electrons. The "fast" group, which retain much of the energy from the cathode fall, are characterized by a large electron temperature. The "slow" group, which grow in

49

number as the beam-like particles become thermalized, would correspond to a smaller temperature. In this study, argon is found to be sensitive to the fast electrons, while cesium is more affected by the slower electrons.

To facilitate future study, the following recommendations concerning the apparatus are proposed:

(1) One limiting factor on the diode operation was a tendency for the discharge to jump to the inside walls of the stainless steel system, particularly to the welded joints. This could be offset by moving the electrodes closer together or by using a larger stainless steel structure. Using glass instead of steel would eliminate this problem altogether.

(2) In order to prevent the cathode from sputtering cesium onto the sapphire windows, the current was kept below 10 mA. A glass shroud placed around the cathode would reduce the sputtering problem and would also discourage the discharge from jumping to the stainless steel wall behind the cathode. However, installing such a shroud might necessitate bring the electrodes in from the side of the cell rather than from the top.

(3) The considerable thermal "inertia" of the stainless steel cell led to a wait of several days as the system was brought to a stable temperature of 250°C. From this standpoint, a quickly heating glass system,

would be preferable. However, glass does not distribute heat as evenly as the stainless steel.

(4) The time spent in changing the cesium pressure could be reduced if the cesium reservoir were moved closer to the electrode gap. At the reservoir location depicted in Figure 5, it is a several hour process for the cesium to distribute itself evenly throughout the cell volume.

The following recommendations concern the experimental and analytical approach:

(1) The argon spectral emission data can be made more complete if the 300-500 nm range is scanned.

(2) The accuracy of this method can not be improved until literature values with smaller uncertainties can be found for transition probabilities, absorption oscillator strengths, and excitation cross sections for both argon and cesium.

(3) The calibration of the spectrometer was not done in absolute units. Hence, measured intensities are only useful when they are compared to one another. It is suggested that, in future studies, an absolute cali-bration be made. This would be useful in determining the number densities of the gas species (Ref. 17:997).

Appendix A: Estimating the Integral in the Calculation of the Average Rate of Electron Impact Excitation

We begin with the following integral:

$$I = \int_0^\infty R_{EXC} \, E^{\frac{1}{2}} \, e^{-E/kT_E} \, dE$$

As noted in the text, the overlap between $E^{1/2}\exp(-E/kT_E)$ and R_{exc} is small. Since R_{exc} and $E_{1/2}$ are slowly varying functions in this region, they may be approximated by linear functions whose slopes are given by the slopes of the original functions at $E=E_{TH}$. This suggests redefining the coordinate origin to $E=E_{TH}$, and defining a new coordinate E^*, where $E^*=(E-E_{TH})/kT_E$. Hence, the linear approximations to R_{exc} and $E_{1/2}$ may be written as

$$H_1(E^*) = \left(kT_E E^* + E_{TH}\right)^{\frac{1}{2}} \approx M_1 E^* + B_1$$

$$H_2(E^*) = R_{EXC} \approx M_2 E^* + B_2$$

where M1, M2 are the slopes and B1, B2 are the ordinate intercepts. These are given by

$$M_1 = \left.\frac{\partial H_1}{\partial E^*}\right|_{E^*=0} = \left.\frac{kT_E}{2}\left(kT_E E^* + E_{TH}\right)^{-\frac{1}{2}}\right|_{E^*=0} = \frac{kT_E}{2\sqrt{E_{TH}}}$$

$$M_2 = \left.\frac{\partial H_2}{\partial E^*}\right|_{E^*=0} = \left.\frac{\partial R_{EXC}}{\partial E^*}\right|_{E^*=0} = \left.kT_E \frac{\partial R_{EXC}}{\partial E}\right|_{E=E_{TH}}$$

$$B_1 = \left.H_1\right|_{E^*=0} = \sqrt{E_{TH}}$$

$$B_2 = \left.H_2\right|_{E^*=0} = \left.R_{EXC}\right|_{E=E_{TH}} = 0$$

Pulling this together, we have the following linear approximations

$$H_1(E^*) = \frac{kT_E}{2\sqrt{E_{TH}}} + E_{TH}^{\frac{1}{2}} = E_{TH}^{\frac{1}{2}}\left(\frac{kT_E E^*}{2 E_{TH}} + 1\right)$$

$$H_2(E^*) = \left(\frac{\partial R_{EXC}}{\partial E}\right)\Bigg|_{E=E_{TH}} E^* kT_E$$

So the integral may be rewritten as

$$\mathbb{I} = \int_0^\infty H_1(E^*) H_2(E^*) e^{-(kT_E E^* + E_{TH})/kT_E} kT_E dE^*$$

$$= E_{TH}^{\frac{1}{2}} \frac{\partial R_{EXC}}{\partial E}\Bigg|_{E=E_{TH}} e^{-E_{TH}/kT_E}(kT_E)^2 \int_0^\infty E^*\left(\frac{kT_E E^*}{2 E_{TH}} + 1\right) e^{-E^*} dE^*$$

Going only to first order in kT_E/E_{TH}, since $kT_E \ll E_{TH}$, the integral becomes

$$\mathbb{I} = E_{TH}^{\frac{1}{2}} e^{-E_{TH}/kT_E} \frac{\partial R_{EXC}}{\partial E}\Bigg|_{E=E_{TH}} (kT_E)^2$$

53

Appendix B: Plots of G(E) vs E for Argon and Cesium
Spectral Emission Data at Various Spatial Locations

54

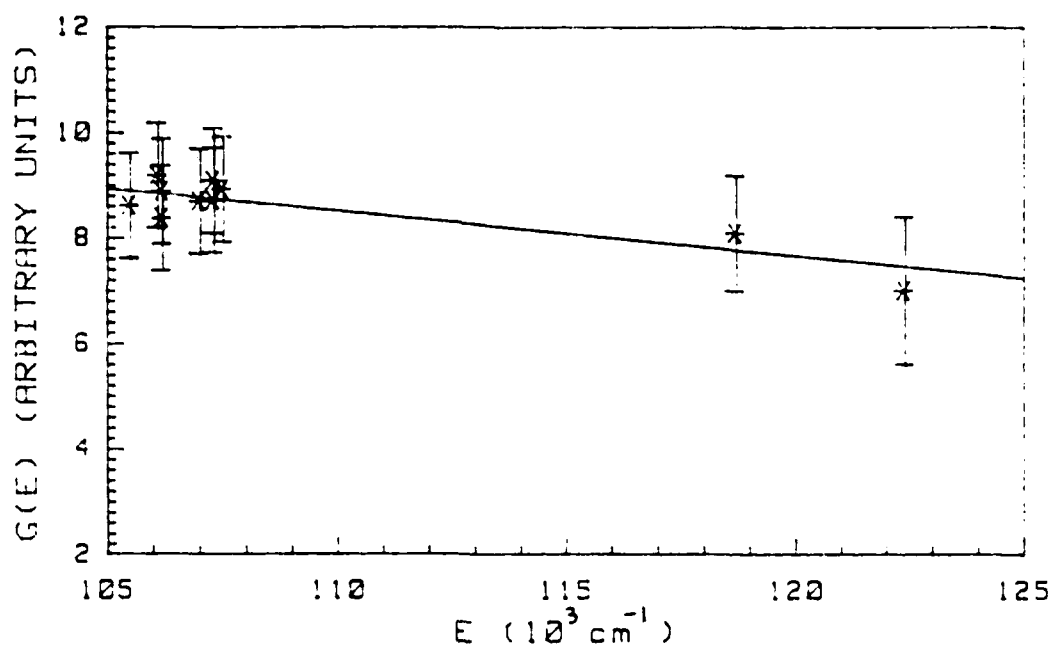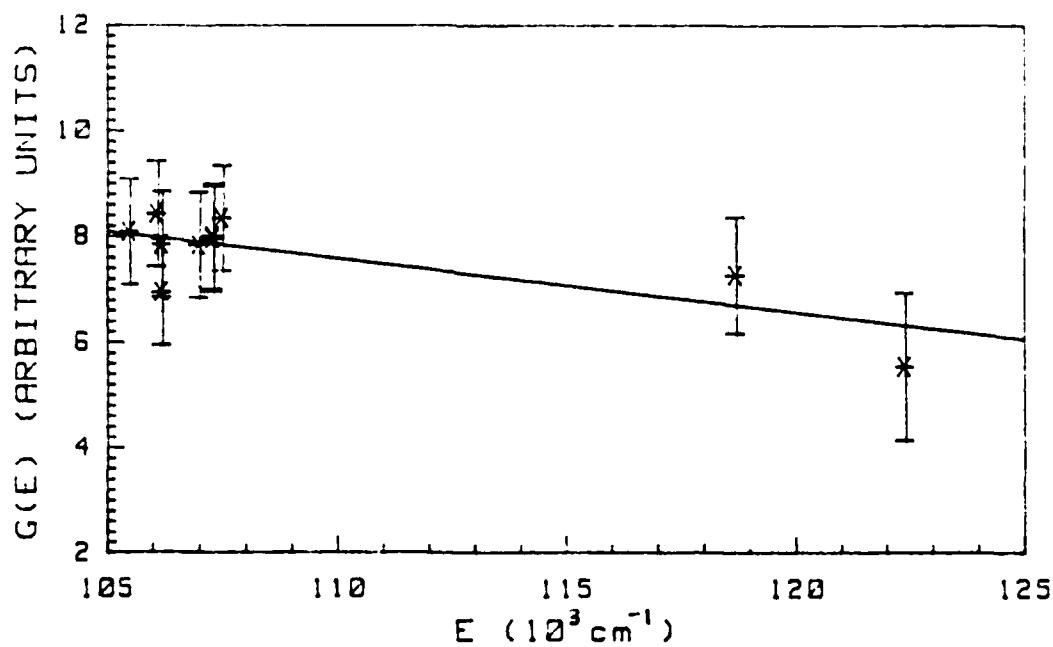FIG.13:Ar TRANSITIONS AT 3.18 mm FROM CATHODE

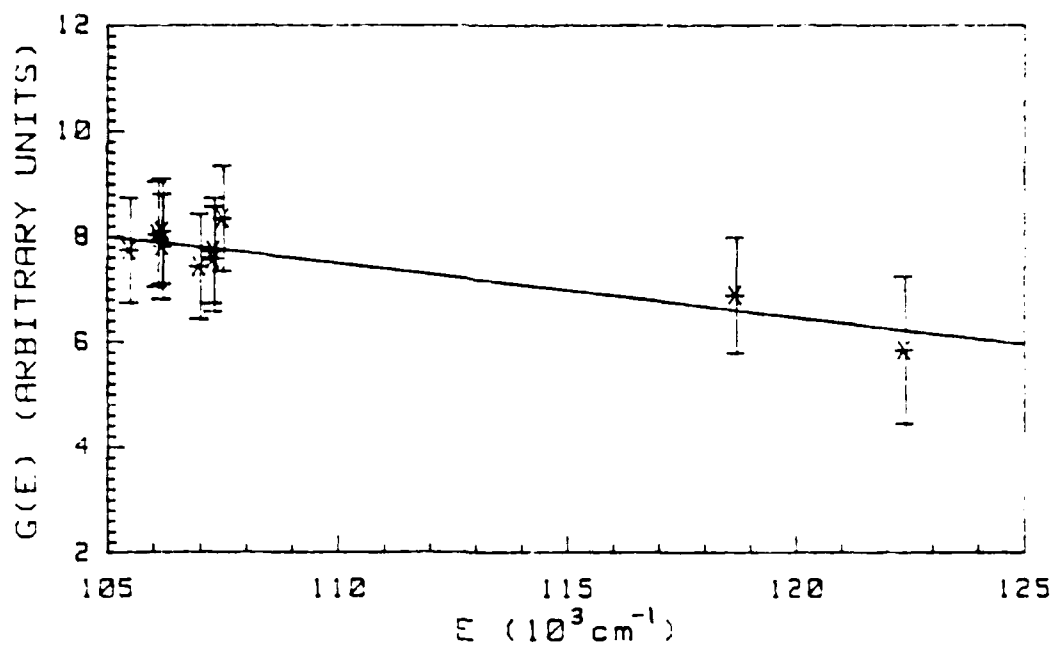FIG.14:Ar TRANSITIONS AT 4.45 mm FROM CATHODE

FIG.15:Ar TRANSITIONS AT 5.72 mm FROM CATHODE
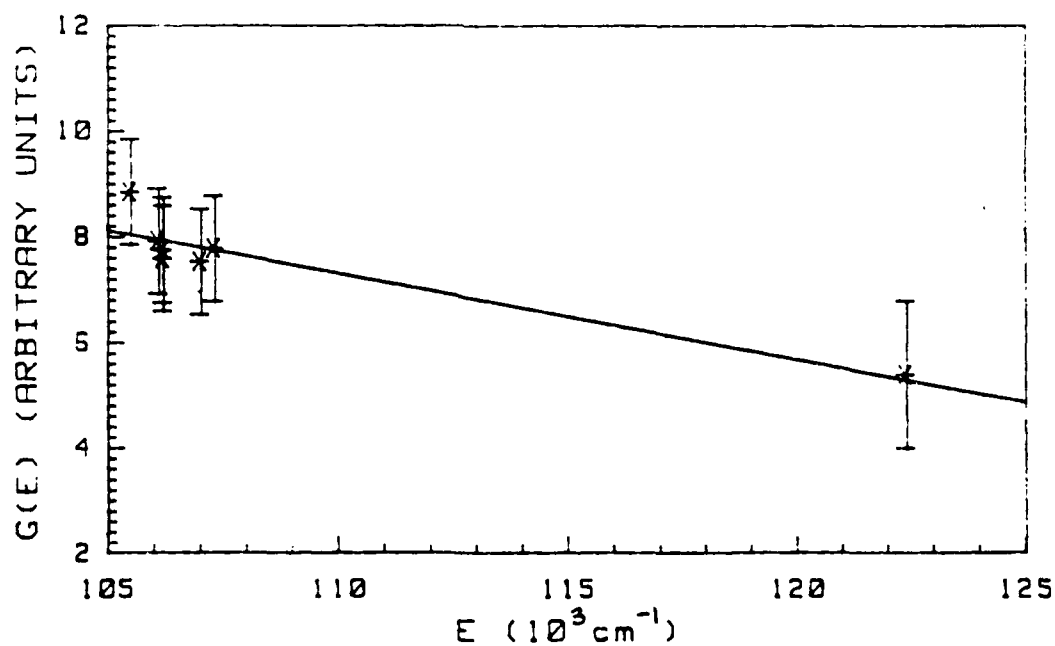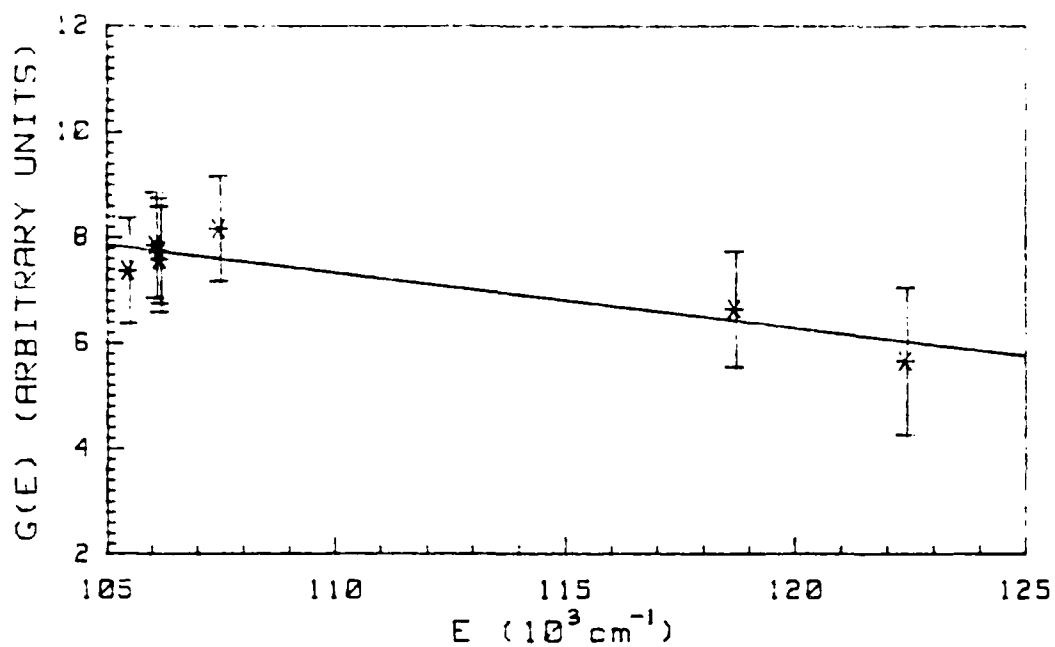

FIG.16:Ar TRANSITIONS AT 6.99 mm FROM CATHODE
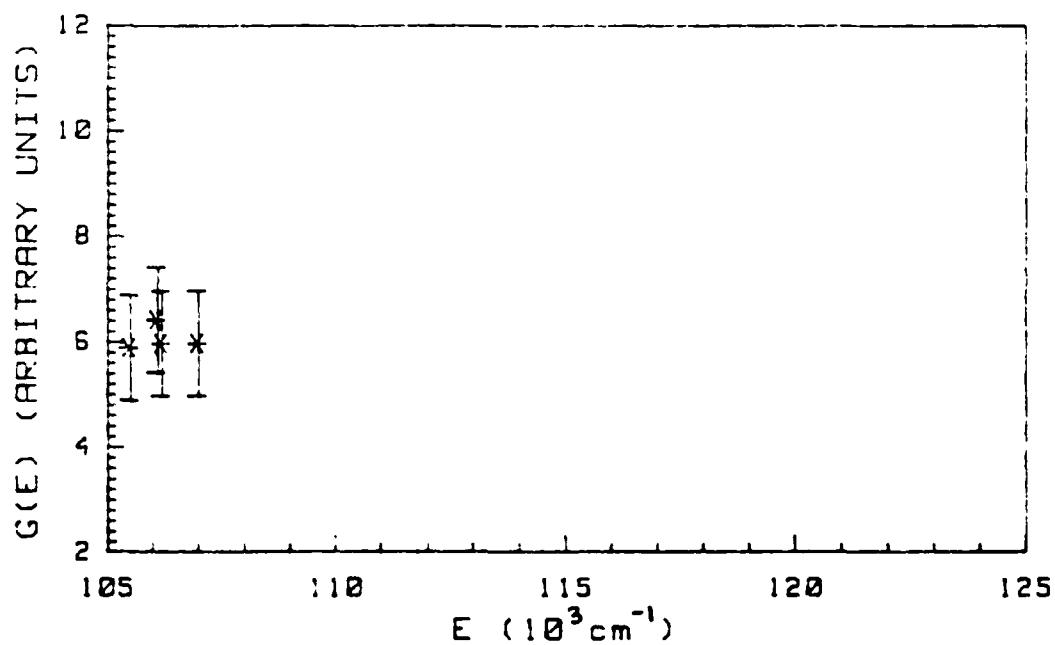
56

FIG.17:Ar TRANSITIONS AT 8.26 mm FROM CATHODE
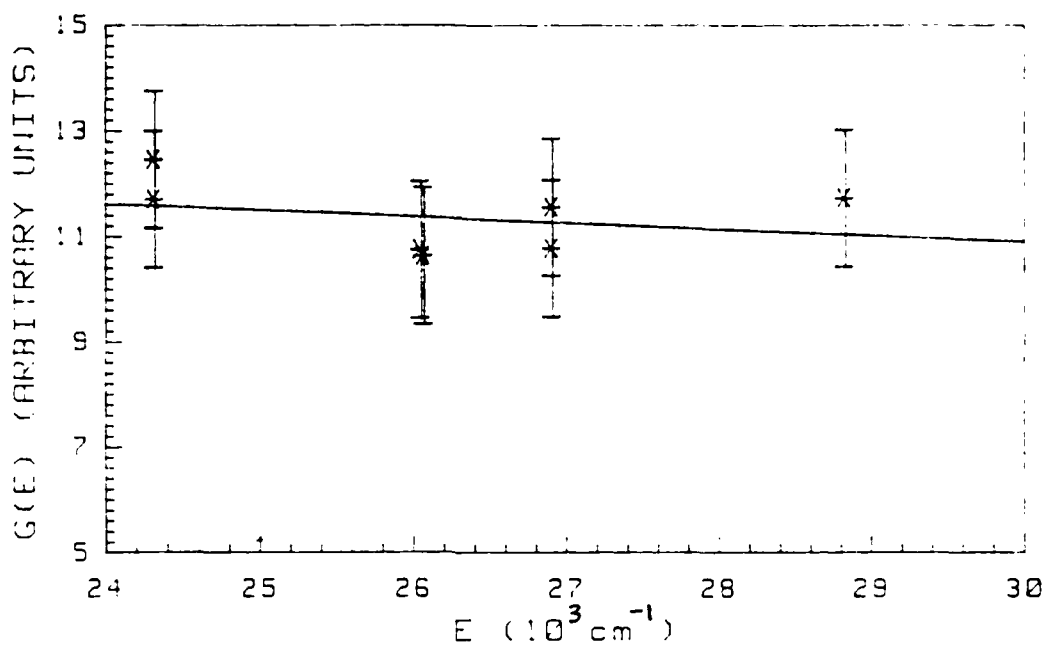

FIG.18:Ar TRANSITIONS AT 13.34 mm FROM CATHODE
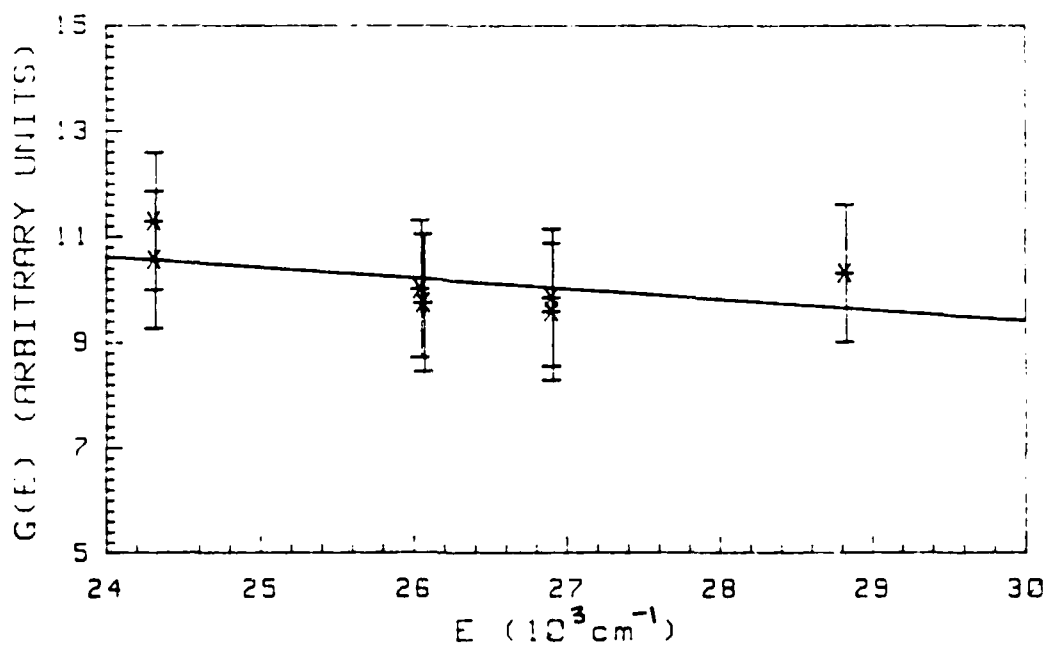
FIG.19:Cs TRANSITIONS AT 3.18 mm FROM CATHODE
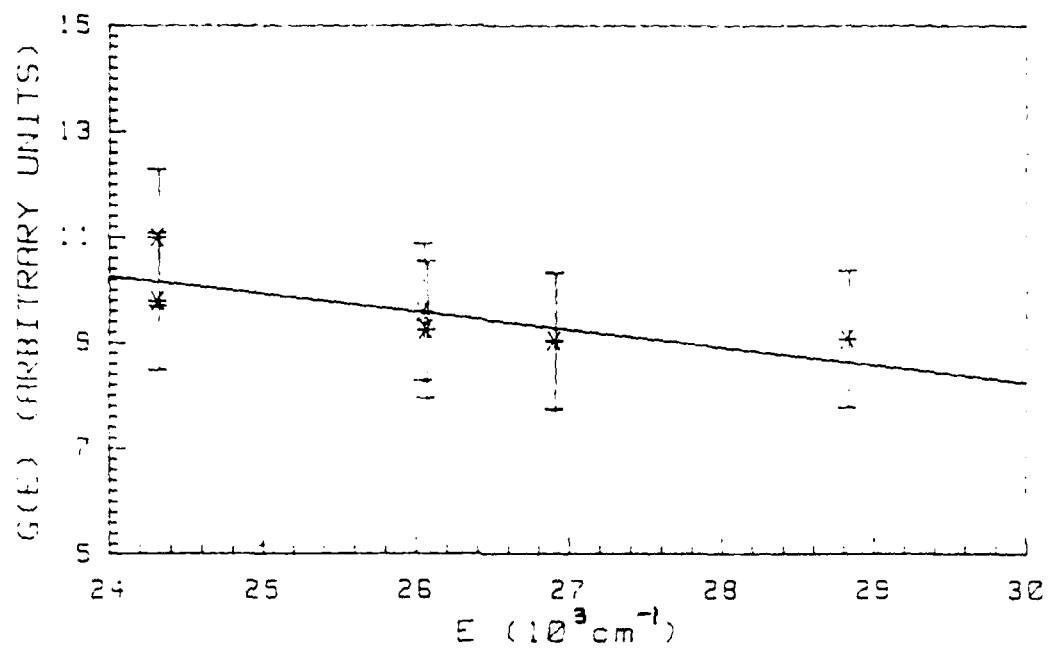

FIG.20:Cs TRANSITIONS AT 4.45 mm FROM CATHODE

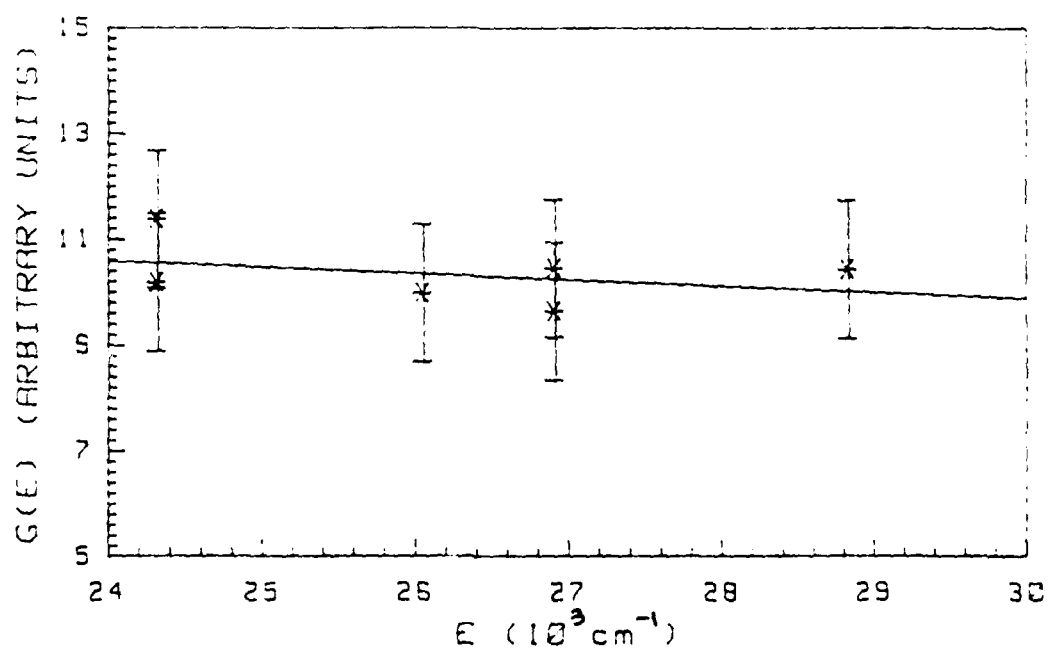FIG.21:Cs TRANSITIONS AT 5.72 mm FROM CATHODE

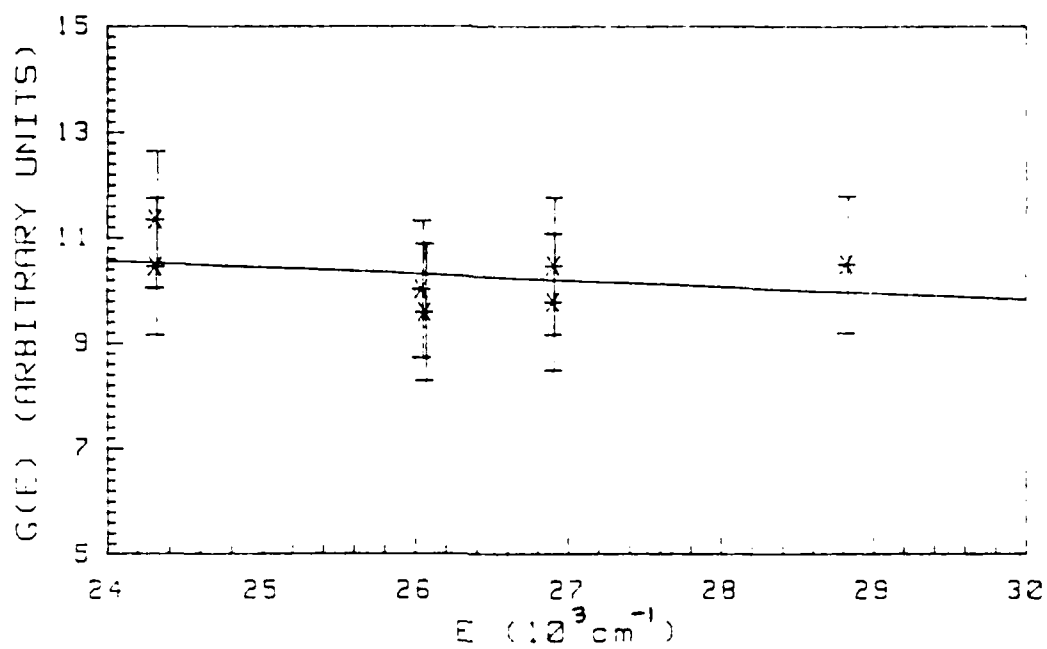FIG.22:Cs TRANSITIONS AT 6.99 mm FROM CATHODE

59
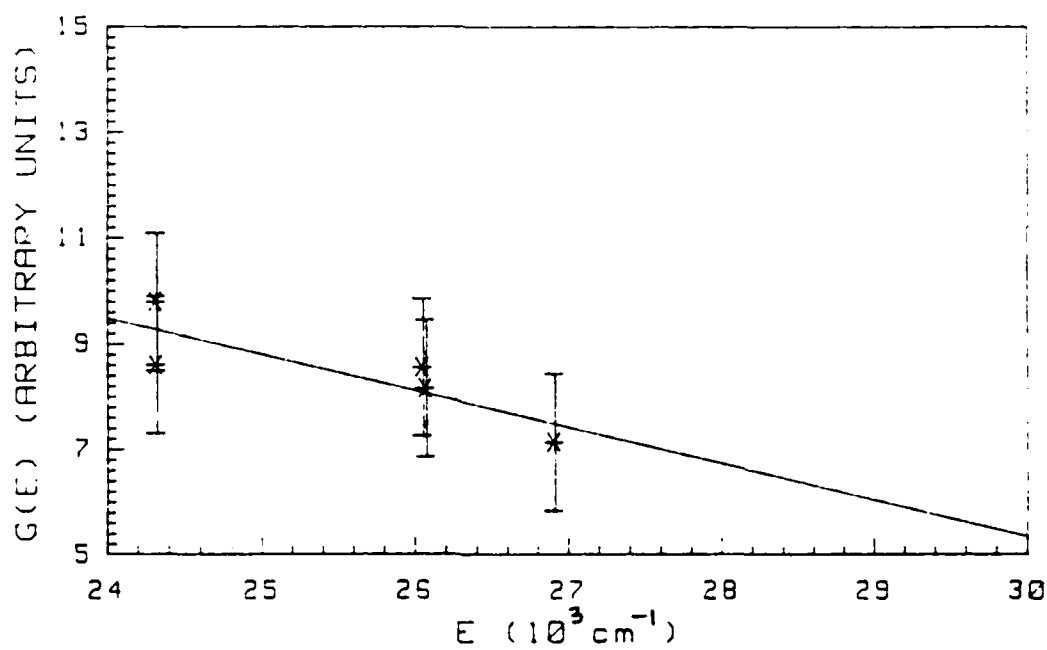
FIG.23:Cs TRANSITIONS AT 8.26 mm FROM CATHODE

FIG.24:Cs TRANSITIONS AT 13.34 mm FROM CATHODE

Bibliography

1. von Engel, A. _Ionized Gases_, Oxford University Press, London, 217, (1965).

2. van Gorcum, A.H. Physica, Haag, $\underline{3}$:207 (1936).

3. Brewer, A.K. and J.W. Westhaver. Jour. App. Phys., 8:779 (1937).

4. Zapesochnyi, I.P., P.V. Feltsan. _Opt. Spect._, $\underline{20}$:291 (1966).

5. Zapesochnyi, I.P., L.L. Shimon. _Opt. Spect._, $\underline{20}$:421 (1965).

6. Zapesochnyi, I.P. _High Temp._, $\underline{5}$:6 (1967).

7. Zapesochnyi, I.P., L.L. Shimon. Opt. Spect., $\underline{16}$:504 (1964).

8. Drawin, H.W. "Atomic Cross-Sections for Inelastic Electronic Collisions," Report EUR-CEA-FC236, (1963).

9. Mitchner, M., C.H. Kruger. _Partially Ionized Gases_, John Wiley and Sons, New York, 27, (1973).

10. Petersen, L.R., J.E. Allen Jr. Jour. Chem. Phys., $\underline{56}$:6068 (1972).

11. Wiese, W.L., _et al._ _Transition Probabilities_, vol. 2. National Standard Reference Data System-National Bureau of Standards 22, 192, (1968).

12. Bailey, W.F. Air Force Institute of Technology. Private discussions. Air Force Institute of Technology, Wright-Patterson A.F.B., OH, Oct-Nov 1987.

13. Bioni, M.A. "Recombination," _Principles of Laser Plasmas_, ed. G. Bekefi, John Wiley and Sons, New York, (1976).

14. Fabry, M., J.R. Cussenot. _Can. Jour. Phys._, $\underline{54}$:836 (1976).

15. Stone, P.M. _Phys. Rev._, $\underline{127}$:1151 (1962).

16. Honig, R.E. "Vapor Pressure Data for the Elements," _The Characterization of High-Temperature Vapors_, ed. J.L. Margrave, John Wiley and Sons, New York 475 (1967).

17. Robinson, D.R., P.D. Lenn. _App. Opt._, $\underline{6}$:983 (1967).

VITA

Lieutenant Michael J. Ward was born on 29 July 1964 in Hollywood, California. He graduated from high school in Newbury Park, California in 1982 and attended Harvey Mudd College in Claremont, California until May 1986, at which time he received the degree of Bachelor of Science in Physics. Upon graduation, he received a commission in the USAF through ROTC Detachment 060. He entered the School of Engineering, Air Force Institute of Technology, in June 1986.

Permanent Address: 4411 Burkhardt Ave., Apt. A7
Dayton, OH 45431

REPORT DOCUMENTATION PAGE

Form Approved
OMB No. 0704-0188

1a. REPORT SECURITY CLASSIFICATION	1b RESTRICTIVE MARKINGS
UNCLASSIFIED	

2a. SECURITY CLASSIFICATION AUTHORITY	3. DISTRIBUTION/AVAILABILITY OF REPORT
	Approved for public release;
2b. DECLASSIFICATION/DOWNGRADING SCHEDULE	distribution unlimited.

4. PERFORMING ORGANIZATION REPORT NUMBER(S)	5. MONITORING ORGANIZATION REPORT NUMBER(S)
AFIT/GE/GEP/87D-9	

6a. NAME OF PERFORMING ORGANIZATION	6b. OFFICE SYMBOL (If applicable)	7a. NAME OF MONITORING ORGANIZATION
School of Eng.	AFIT/ENG	

6c. ADDRESS (City, State, and ZIP Code)	7b. ADDRESS (City, State, and ZIP Code)
Air Force Institute of Technology Wright-Patterson AFB, OH 45433-6583	

8a. NAME OF FUNDING/SPONSORING ORGANIZATION	8b. OFFICE SYMBOL (If applicable)	9. PROCUREMENT INSTRUMENT IDENTIFICATION NUMBER
AF Wright-Aero. Prop. Lab Adv. Plasma Research Gp.	AFWAL/POOC-3	

8c. ADDRESS (City, State, and ZIP Code)	10. SOURCE OF FUNDING NUMBERS			
	PROGRAM ELEMENT NO.	PROJECT NO.	TASK NO	WORK UNIT ACCESSION NO.
Air Force Wright-Aero. Propulsion Lab Wright-Patterson AFB, OH 45433-5000				

11. TITLE (Include Security Classification)
ELECTRON TEMPERATURE MEASUREMENTS IN AN ARGON/CESIUM PLASMA DIODE (UNCLASSIFIED)

12. PERSONAL AUTHOR(S)
Ward, Michael J., B.S., 2d Lt, USAF

13a. TYPE OF REPORT	13b. TIME COVERED	14. DATE OF REPORT (Year, Month, Day)	15. PAGE COUNT
MS Thesis	FROM _____ TO _____	1987 December	71

16. SUPPLEMENTARY NOTATION

Approved for public release: IAW AFR 190-1
LYNN E. WOLAVER 31 Dec 87
Dean for Research and Professional Development
Air Force Institute of Technology (AFIT)

17. COSATI CODES			18. SUBJECT TERMS (Continue on reverse if necessary and identify by block number)
FIELD	GROUP	SUB-GROUP	Plasma Diagnostics, Electric Discharge, Cesium,
20	9		Spectroscopy, Spectral Lines, Argon,
			Electron Energy

19. ABSTRACT (Continue on reverse if necessary and identify by block number)

Thesis Chairman: William F. Bailey, Professor of Physics.

Line intensity measurements in an argon/cesium plasma diode were made at various locations within the discharge, yielding a spatially resolved electron temperature distribution. This device operated at 0.9 Torr argon, 0.04 Torr cesium, and at a current density of 1.05 mA/cm^2. Observations of the spectral line intensities of the 6P→nS and 6P→nD transitions of cesium yielded an average electron temperature of 8200 K throughout most of the discharge region. In contrast, the argon line emission data yields an average electron temperature of 13500 K. The difference between these two measured "electron temperatures" suggests that the electron energy distribution function is non-Maxwellian under the measured plasma conditions.

20. DISTRIBUTION/AVAILABILITY OF ABSTRACT	21. ABSTRACT SECURITY CLASSIFICATION
☒ UNCLASSIFIED/UNLIMITED ☐ SAME AS RPT. ☐ DTIC USERS	Unclassified

22a NAME OF RESPONSIBLE INDIVIDUAL	22b. TELEPHONE (Include Area Code)	22c. OFFICE SYMBOL
William F. Bailey	(513) 255-2012	AFIT/ENG

DD Form 1473, JUN 86   Previous editions are obsolete.

END
DATE
FILMD
3 - 88
DTIC